Differential Effects of Proinflammatory Cytokines on TGF-β1-Mediated Biomechanical and Biochemical Properties of 3D Human Fibroblast Tissues

By

Katerina St. Angelo

Bachelor of Science in Biology, Rivier University, 2022

Thesis

Submitted in partial fulfillment of the requirements for the Degree of Master of Science in the Graduate Program of Biotechnology at Brown University

PROVIDENCE, RHODE ISLAND

May 2026

This thesis by Katerina St. Angelo is accepted in its present form by the Graduate Program in Biotechnology as satisfying the thesis requirements for the degree of Master of Science

Date 4/15/26 Signature: _____

Dr. Jeffrey Morgan, Advisor

Date 4/15/2026 Signature: _____

Dr. Diana Horrigan, Reader

Date 4/17/2026 Signature: _____

Dr. Jacquelyn Schell, Reader

Approved by the Graduate Council

Date _____ Signature: _____

Dr. David P. Lindstrom, Dean of the Graduate School

Acknowledgments

I would like to express my sincere gratitude to the Brown University community for their support throughout my master's studies. First and foremost, I would like to thank my advisor, Dr. Jeffrey Morgan, for welcoming me into his lab and for his mentorship, guidance, and continued support throughout this research project. His insight and encouragement were invaluable to my academic and professional development. I would also like to thank Dr. Jacquelyn Schell, the program director, for her guidance, support, and thoughtful feedback throughout my time in the program and during the completion of this thesis.

I would like to thank Madeline Marx for being a supportive and dedicated member of the lab and a true friend throughout this process. Her collaboration and encouragement were greatly appreciated.

I am deeply grateful to my parents, Gerald and Melissa, for their unwavering love, support, and encouragement throughout my academic journey. Their belief in me and constant reassurance made even the most challenging moments feel manageable. I would also like to thank my fiancé, Andrew, for his patience, understanding, and endless support throughout this process. His encouragement and presence were a constant throughout this process.

Lastly, I would like to thank my siblings and their spouses, as well as my niece and nephews, and the friends who meant so much to me throughout my graduate studies. During the completion of this thesis, I experienced the loss of my grandmother, Evie, and my dog, Merc, who were both a significant part of my life. My grandmother played a profound role in shaping the person I am today, and her influence continues to guide me as I move forward into the next chapter of my life following the completion of this thesis.

Table of Contents

Table of Figures

Table of Tables

Abstract of Differential Effects of Proinflammatory Cytokines on TGF-β1-Mediated Biomechanical and Biochemical Properties of 3D Human Fibroblast Tissues, by Katerina St. Angelo, ScM, Brown University, May 2026

ABSTRACT

Fibrosis is driven by excessive extracellular matrix (ECM) deposition and is a hallmark of chronic diseases including pulmonary fibrosis, liver cirrhosis, and cardiac fibrosis. TGF-β1 is the primary driver of fibroblast activation, promoting myofibroblast differentiation, collagen synthesis, and increased tissue stiffness. However, the fibrotic environment contains a diverse array of proinflammatory cytokines that may modulate TGF-β1's effects on fibroblasts. To investigate this, we used a scaffold-free 3D *in vitro* ring tissue model in which human fibroblasts self-assemble into a collagen-rich connective tissue over 14 days. Ring tissues were treated with TNF-α, IL-18, IL-1β, IFN-γ, or IL-1α, alone and in combination with TGF-β1. Tissue size, total DNA, total collagen, biomechanical properties (ultimate tensile strength and maximum tangent modulus), and histology were assessed at days 7 and 14. TGF-β1 increased collagen accumulation and the strength and stiffness of ring tissues. TNF-α, IL-1β, and IL-1α each reduced tissue size, total collagen, and the tensile strength and stiffness of both control and TGF-β1-stimulated tissues, effectively counteracting TGF-β1-mediated collagen accumulation. Histological analysis revealed that TNF-α and IL-1β disrupted collagen fiber architecture and increased nuclear pyknosis, effects that were most pronounced in TGF-β1-stimulated tissues. In contrast, IL-18 and IFN-γ had little to no effect on collagen accumulation or tissue mechanics in either control or TGF-β1-stimulated tissues. These findings demonstrate that proinflammatory cytokines have divergent effects on fibroblast-mediated collagen deposition: TNF-α, IL-1β, and IL-1α act as counter regulators of TGF-β1-driven fibrosis, while IL-18 and IFN-γ are largely neutral in this context. This work highlights the complexity of cytokine crosstalk in fibrosis and demonstrates the utility of 3D *in vitro* tissue models for dissecting cytokine-specific contributions to collagen accumulation and

tissue biomechanics.

Introduction

Fibrosis and Inflammatory Regulation of Extracellular Matrix Remodeling

Fibrosis is a pathological condition characterized by excessive extracellular matrix (ECM) deposition and progressive tissue scarring, and it underlies a wide range of chronic diseases, including pulmonary fibrosis, liver cirrhosis, renal fibrosis, and cardiac fibrosis [1,2,3]. Across organ systems, fibrosis represents a maladaptive wound healing response that arises from persistent or dysregulated tissue injury and repair mechanisms. While acute wound healing is a tightly coordinated and self-limiting process, chronic injury disrupts this balance, leading to sustained matrix deposition, architectural distortion, and ultimately organ dysfunction and failure [1,2,3]. Given its contribution to morbidity and mortality worldwide, understanding the cellular and molecular mechanisms that drive fibrotic progression remains a critical biomedical challenge.

A central feature of fibrosis is the interplay between inflammation and fibroblast activation. Inflammatory signaling and cytokine-mediated communication between immune cells and resident stromal cells initiate and perpetuate fibrotic remodeling [4,5,6,7]. Following tissue injury, immune cells release a diverse array of cytokines and growth factors that alter fibroblast phenotype, promoting proliferation, migration, and differentiation into activated, matrix-producing cells. Within fibrotic tissues, pro-inflammatory and anti-inflammatory cytokines form a tightly interconnected signaling network whose balance ultimately determines whether injury resolves or progresses toward chronic fibrosis. Although inflammation acts as a key upstream regulator, it is ultimately the sustained activation of fibroblasts that drives excessive synthesis and accumulation of collagen-rich ECM, leading to increased tissue stiffness, loss of normal architecture, and progressive functional decline.

Despite significant advances in identifying pro-fibrotic cytokines and signaling pathways, much of our understanding of fibroblast activation has been derived from two-dimensional culture systems that fail to fully recapitulate the structural and mechanical complexity of native tissue. Fibroblast behavior is highly context-dependent, and matrix organization, cell–cell interactions, and mechanical loading conditions all influence cytokine responsiveness and ECM deposition. In fibrotic disease, alterations in collagen architecture and tissue stiffness further reinforce fibroblast activation through mechanotransductive signaling, creating a feed-forward relationship between inflammation, matrix remodeling, and mechanical dysfunction. Therefore, experimental models that incorporate three-dimensional structure and allow for functional mechanical assessment are essential for studying how defined cytokine environments regulate ECM maturation and tissue-level properties. To address this need, we utilize an engineered three-dimensional fibroblast ring model that enables controlled modulation of cytokine conditions while quantitatively assessing collagen deposition and biomechanical function.

3D *In Vitro* Ring Microtissue

Building on previous work from the Morgan Lab, we developed a 3D *in vitro* model of a collagen-rich connective tissue to investigate how various cytokines influence development[8,9]. In this system, human fibroblasts are seeded into 5mm circular agarose troughs where they self-assemble and form a stable ring-shaped tissue. Over a four-week period, these tissues generate a robust, collagen-dense extracellular matrix entirely independent of artificial scaffolding. Consistent with *in vivo* fibrotic progression, TGF-β1 was found to drive collagen synthesis and significantly enhance the mechanical integrity, specifically the strength and stiffness, of the 3D fibroblast rings. This model has been used to show that TGF-β1 alone cannot sustain collagen production and subsequent increases in tensile properties. Previous findings indicate that the

sustained elevation of these tensile properties is dependent on the presence of IL-13, an immune-cell-derived cytokine [10].

The Role of Extracellular Matrix in Tissue Biomechanics

The extracellular matrix (ECM) of human fibroblast tissues is a dynamic, non-cellular network that provides structural support while also regulating cellular behavior through biochemical and mechanical signaling [11,12]. In this model, collagen-based structures comprise approximately 80% of the total ECM, with the remaining portion consisting of resident fibroblasts and other cellular components embedded within the matrix [8,9]. These collagen fibers assemble into complex, multilayered, and crosslinked fibrillar networks that form the structural backbone of connective tissues and largely determine their mechanical integrity [13]. In addition to collagen, ECM components such as elastin and fibronectin contribute to elasticity and cell–matrix adhesion, respectively, allowing fibroblasts to sense and respond to their microenvironment through integrin-mediated signaling pathways [14] **(Figure 1)**. Because fibroblasts both produce and remodel the ECM, alterations in cytokine signaling can directly influence matrix deposition, organization, and crosslinking, ultimately impacting tissue-level mechanical properties[11,12].

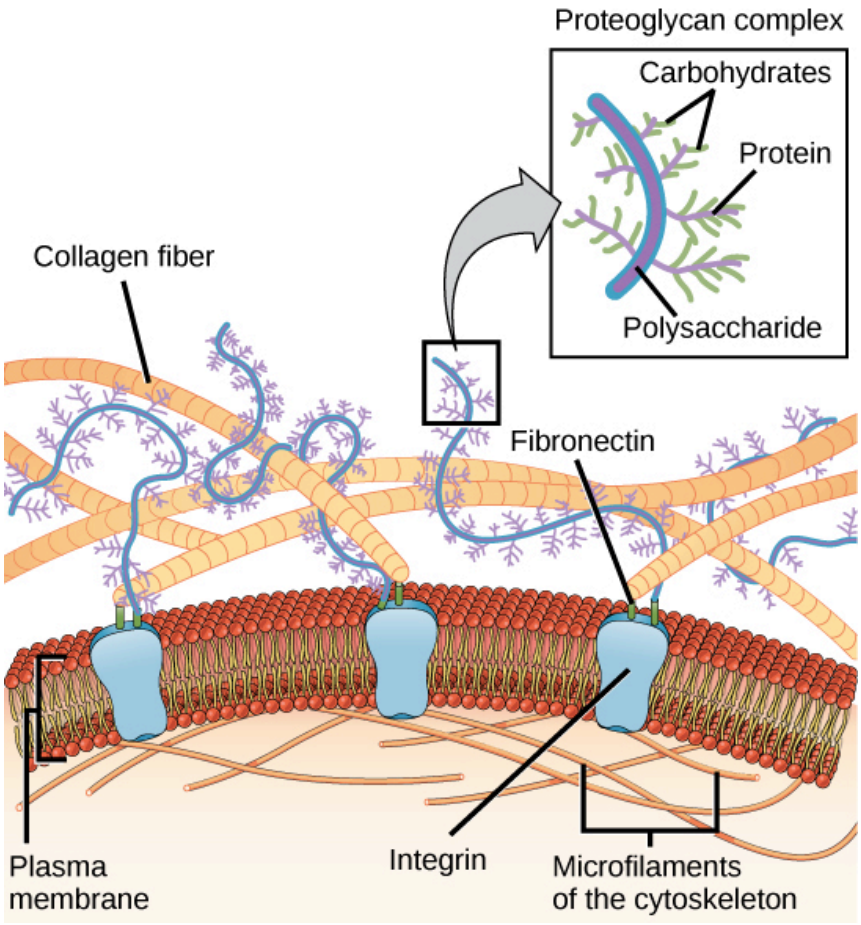

Figure 1: Extracellular matrix (ECM) composition. The ECM is primarily composed of structural proteins, including collagen, elastin, and fibronectin. Collagen is the most abundant component and provides structural support and tensile strength to tissues. Elastin is a glycoprotein that imparts elasticity, allowing tissues to stretch and return to their original shape. Fibronectin is a glycoprotein that binds to integrin receptors on the plasma membrane, facilitating cell adhesion to the ECM. Bose et al. [15]

To quantify these functional properties in engineered ring tissues, mechanical analysis is performed using principles grounded in Hooke's Law and Young's modulus, which describe the proportional relationship between applied force and resulting deformation within the linear elastic region [16]. When an external force is applied, the internal matrix resists that force,

generating stress, defined as force divided by cross-sectional area (MPa) [16]. The resulting deformation is described as strain, calculated as the change in length divided by the original length [16]. Plotting stress versus strain generates a stress–strain curve that characterizes tissue behavior under load **(Figure 2)**[16]. From this curve, key mechanical parameters can be derived, including maximum tangent modulus (MTM), which reflects tissue stiffness and corresponds to the slope of the linear region, and ultimate tensile strength (UTS), which represents the maximum stress the tissue can withstand prior to failure[16]. The overall shape of the stress–strain curve also provides insight into whether the tissue exhibits brittle, plastic, or ductile behavior [16]. In the context of cytokine-modulated ECM remodeling, shifts in collagen deposition, matrix organization, or fibroblast contractility are expected to alter MTM and UTS, thereby providing a functional readout of cytokine-driven changes in matrix maturation [11,12].

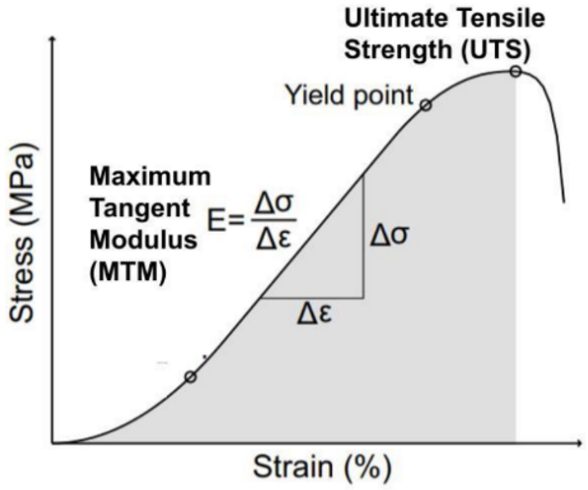

Figure 2: Representative stress–strain curve illustrating fundamental mechanical properties of a material. Stress is defined as the force applied per unit cross-sectional area, while strain represents the relative deformation of the material. The peak of the curve corresponds to the ultimate tensile strength (UTS), the maximum stress the material can withstand before fracture. The yield point indicates the elastic limit, beyond which permanent deformation occurs. Below the yield point, the slope of the linear region reflects the material's stiffness and corresponds to Young's modulus of elasticity. Figure from Ristaniemi et al. [16]

Transforming growth factor- beta-1 (TGF-β1): Primary Driver of Fibroblast Activation

Transforming growth factor-beta-1 (TGF-β1) is widely recognized as the master regulator of fibroblast activation and the primary driver of the fibrotic process. Under the influence of TGF-β1, resident fibroblasts undergo a phenotypic transition into myofibroblasts, which are specialized contractile cells characterized by the expression of alpha-smooth muscle actin (α-SMA) and an increased capacity for collagen synthesis. This activation is the hallmark of fibrotic

progression, leading to the excessive accumulation of extracellular matrix components that compromise tissue function [11,17,44]. While TGF-β1 provides the fundamental drive for this remodeling, its effects are often context-dependent and influenced by the surrounding inflammatory environment[12]. This established role for TGF-β1 serves as the benchmark for this study, allowing for a direct comparison of how other inflammatory cytokines modulate the standard fibrotic response.

Proinflammatory Modulators of Fibrotic Progression

While TGF-β1 provides the essential stimulus for myofibroblast differentiation, the fibrotic environment is composed of a diverse array of proinflammatory cytokines that actively shape the remodeling process. These factors do not act in isolation, rather, they engage in a complex biochemical dialogue with resident fibroblasts, often converging on the same intracellular signaling. This study investigates the individual and synergistic roles of Tumor Necrosis Factor-alpha (TNF-α), Interleukin-18 (IL-18), Interleukin-1 beta (IL-1β), Interferon gamma (IFN-γ), and Interleukin-1 alpha (IL-1α). By examining these specific mediators, we aim to gain a better understanding of how the inflammatory environment dictates the transition from acute repair to chronic, maladaptive fibrosis. Each of these cytokines contributes a unique regulatory input, collectively determining the mechanical and structural fate of the maturing tissue.

Tumor necrosis factor-alpha (TNF-α): Inhibitor of Collagen synthesis

Tumor Necrosis Factor-alpha (TNF-α) is a central coordinator of the early inflammatory response and is noted for its complex interaction with TGF-β1. While it is a potent driver of myofibroblast contractility, TNF-α has also been shown to contradict the repression of collagen

production typically induced by TGF-β1 [18]. This biochemical crosstalk interferes with the signaling that drives matrix gene expression. Consequently, TNF-α is thought to dictate the inflammatory processes, shifting the fibroblast from a purely matrix-producing cell to one that actively maintains a state of chronic tissue tension and inflammatory signaling [17,18].

Interleukin-18 (IL-18) and Interleukin-1 beta (IL-1β): Enhancers of the Fibrotic Response

The IL-1 family members, IL-18 and IL-1β, serve as critical biochemical links between acute tissue injury and sustained remodeling. Both cytokines are typically released following the activation of the NLRP3 inflammasome, a sensor for cellular danger and stress [19]. Rather than acting as independent drivers of collagen synthesis, these cytokines are recognized for their ability to prepare the stromal environment for remodeling. This process increases the sensitivity of resident fibroblasts to TGF-β1 and encourages the transition into a highly contractile myofibroblast phenotype [19,20].

Interferon gamma (IFN-γ): Suppressor of Fibrotic Signaling

In contrast to the pro-fibrotic nature of the TNF and IL-1 families, Interferon gamma (IFN-γ) functions as a pivotal inhibitor of the fibrotic process. Primarily secreted by immune cells, IFN-γ initiates a signaling cascade that actively interferes with the TGF-β1 pathway. This anti-fibrotic effect is largely mediated by the induction of inhibitory proteins, such as Smad7, which prevent pro-fibrotic signals from reaching the nucleus and driving gene expression [21]. By suppressing collagen synthesis and promoting the expression of matrix-degrading enzymes, IFN-γ serves as a critical regulatory check within the tissue.

Interleukin- 1 alpha (IL- 1α): Driver of Early Fibroblast Activation

Finally, Interleukin-1 alpha (IL-1α) represents a unique alarmin signal released rapidly upon cell damage to signal immediate environmental stress[22]. Like IL-1β, IL-1α signals through the IL-1 receptor (IL-1R1), activating downstream NF-κB and MAPK pathways, which may drive similar effects on fibroblast-mediated collagen production[22]. Within the fibrotic tissue, IL-1α acts as an early stimulus that prepares resident fibroblasts for subsequent collagen deposition. Its presence at the site of injury provides an immediate inflammatory signal that sets the stage for TGF-β1-mediated matrix deposition and the subsequent mechanical changes that occur during the initial stages of tissue repair.

This study investigates how proinflammatory cytokines individually and collectively modulate TGF-β1-driven ECM remodeling in a scaffold-free 3D *in vitro* ring tissue model. The drug treatment groups being studied are untreated control, TNF-α, IL-18, IL-1β, IFN-γ and IL-1α. All these treatment groups are also being studied in the context of TGF-β1, those groups are as follows: TGF-β1, TNF-α plus TGF-β1, IL-18 plus TGF-β1, IL-1β plus TGF-β1, IFN-γ plus TGF-β1 and IL-1α plus TGF-β1. Brightfield bottom view *(x,y)* images of these treatment groups are taken on days 2, 4, 7 and 14 along with side view *(z)* at day 14. On day 7 and day 14 randomly selected ring tissues are saved for histology, collagen or DNA measurements. On day 14 rings are selected from each group and measured to determine the effect of each treatment on tissue ring mechanical properties. Together, these measurements allow for a comprehensive assessment of how each cytokine, alone and in combination with TGF-β1, influences fibroblast-mediated collagen accumulation, tissue mechanics, and ECM architecture.

Methods

2D Cell Culture

Cells used for all experiments were juvenile human dermal fibroblast (JNHDF) purchased and expanded from PromoCell, Heidelberg, Germany. These cells were cultured, then expanded and stored in 1mL of DMEM (w/ FBS and Penn/Strep) plus DMSO and stored long term in liquid nitrogen cryotank. For all experiments cells at passage 3 through 6 were thawed and cultured for the following experiments. Cells were cultured in DMEM (Dulbecco's Modified Eagle's Medium)(#11995073, Thermo Fisher Scientific, Grand Island, NY) containing high glucose, L-glutamine, phenol red and sodium pyruvate. This complete media (JNHDF-CM) was also supplemented with 10% fetal bovine serum (FBS)(#100-500, Gemini Bio, Sacramento, CA) and 1% penicillin/streptomycin (#091670249, Thomas Scientific, Swedesboro, NJ). Cells were cultured in T-175 cm^2 (Fisher Scientific, Hampton, NH; catalog #10-126-13) lying flat in an incubator at 37°C and 10% CO_2 . Once cells reached 80-90% confluency, a passage then occurred. For passaging, spent cell culture media was aspirated out of the flask. Cells were then washed with 20 mL of phosphate buffered saline (PBS) (#MT21040CM,Fisher Scientific, Manassas, VA). PBS was then aspirated out of the flask and replaced with 0.05% trypsin (#SH3004201, Thermo Fisher Scientific) in PBS and incubated for 5 minutes. Cells were then removed from the incubator and inspected to ensure that all cells had been liberated from the plastic surface; this was visualized under a Nikon Eclipse TS100 microscope (Nikon, Tokyo, Japan) at 4x magnification. After this confirmation, 20 mL of JNHDF-CM was added to the flask to stop the process of trypsinization. The mixture of cells, trypsin and media was then carefully placed into a 50 mL conical tube and centrifuged at 800 rpm for 6 minutes. Remaining media in the 50 mL conical tube was carefully aspirated out without disturbing the cell pellet. Cells were

resuspended in 5 mL of JNHDF-CM and then counted by adding 10 µl to each side of a hemocytometer. Cells then were passed to a new flask at a density of 5.0 x 10^3 cells/flask. Media was refreshed 3x week and were regularly passaged until P9.

3D Ring Tissue Mold Fabrication

Molds with a circular trough of 5 mm diameter made with 2% agarose were used to grow 3D ring tissues, this method previously described by [23,24]. The molding system was developed using CAD and Solid Works and then produced for prototyping by Protolabs (Maple Plain, MN). Designed and fabricated was a two component stainless steel mold and inserts along with a base to ensure central alignment. These 24-well molds were fabricated to fit on a standard 24-well plate (cat# 3527, Corning). Each well was filled with 1.5mL of 2%(w/v) molten sterile agarose (#BP160-500, Fisher Scientific, Hampton, NH) in PBS. The plastic well dish was placed on a steel plate to lock in each component to ensure each well was centered to the insert. A stainless steel holder, along with individual well inserts were placed into each well and the agarose allowed to cool and gel for up to 15 minutes **(Figure 3)**. After each mold was removed the well contained a molded gel with a 0.75 mm wide cylindrical trough surrounding an agarose peg with a 5 mm diameter. Gels were equilibrated (3x) with serum-free DMEM with 1% penicillin/ streptomycin (SFM) prior to the addition of cells.

Seeding of 3D Ring Tissues

As described previously, cells were liberated from culture flasks and counted[8,9]. After calculating the number of gels to be seeded, a cell density of 300,000 cells per ring was transferred into a new 50 mL conical tube and centrifuged at 800 rpm for 6 minutes. The media was then aspirated off carefully and the cells were resuspended in (75 µl x number of gels) 50:50

media. 50:50 media contained equal parts of serum-free plus (SFM+) and serum-free advanced (SFMA). The SFM+ contains DMEM supplemented with 50 ug/mL L-proline (#BP392-100, Fisher Scientific) and 0.1mM 2-phospho-L-ascorbic acid trisodium salt (#49752, Sigma-Aldrich) and 1% penicillin/streptomycin (#091670249, Thomas Scientific, Swedesboro, NJ). The SFMA contained advanced DMEM (#12491015, Thermo Fisher Scientific) supplemented with 4 mM Glutamax (#35-050-061, Fisher Scientific) and 1% penicillin/streptomycin (#091670249,Thomas Scientific, Swedesboro, NJ). Once cells were resuspended, 75 µl was then added to the trough of each gel **(Figure 3)**. Cells were allowed to settle for 1 hour before slowly adding 1 mL of 50:50 media to each well. Gels were then incubated at 37°C and 10% CO_2 for 24 hours before performing a media change/ drug dosing.

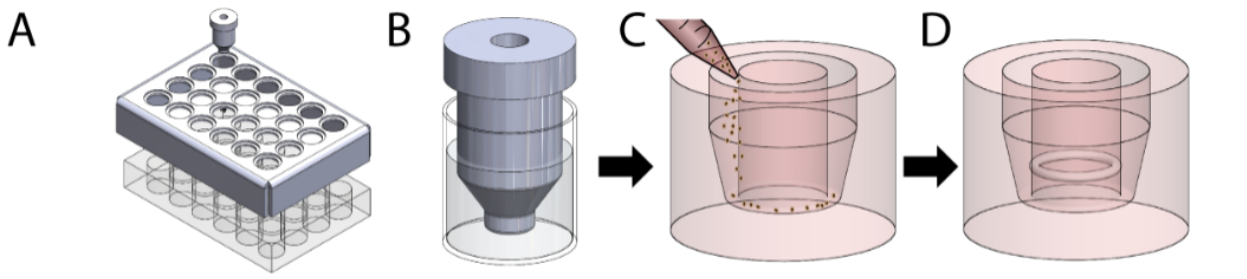

Figure 3 : 3D Ring-Shaped Mold System. 5 mm microtissue rings were formed from the stainless steel mold inserts being placed into the aluminum base surrounding (A, B) a 24 well plate with molten agarose . Those molds were later seeded with JNHDF cells (C) and self-assembled around a central peg which grew for 7 to 14 days (D).

Drug and Growth factor Treatment of 3D Ring tissues

Prior to cytokine addition, rings were allowed to form for 24 hours. TGF-β1(#100-21-50UG, ThermoFisher Scientific), TNF-α (#PHC3015, Fisher Scientific), IL-18 (#PHC0186, ThermoFisher Scientific), IL-1β (200-01B-100UG, Thermo Fisher Scientific), IFN-γ (#I17001, Millipore Sigma) and IL-1α (#200-01A-10UG, Thermo Fisher Scientific) were resuspended and aliquoted according to the manufacturer's protocols. TGF-β1 was reconstituted in 10 mM citric acid, pH 3.0 (Cell Signaling Technologies, #9871L) and diluted in 0.1% (w/v) final concentration of bovine serum albumin (BSA) in PBS. TNF-α was reconstituted in biology grade molecular water (#BP2819-1, Fisher Scientific). IL-18 was reconstituted in 1 M Tris HCL (ThermoFisher Scientific, #15567027). IL-1β was reconstituted in 0.1% (w/v) final concentration of bovine serum albumin (BSA) in PBS. IFN-γ was reconstituted in Molecular Biology Grade Water (Fisher BioReagents, #BP2819). IL-1α was reconstituted in Molecular Biology Grade Water (Fisher BioReagents, #BP2819). Considering that each well had 1.5 ml of agarose and 1 ml of medium that could be removed, growth factors were added to 50:50 medium to achieve a final concentration of 10 ng/mL for TGF-β1, 10 ng/mL for TNF-α, 50 ng/mL for IL-18, 50 ng/mL for IL-1β , 25ug/mL for IFN-γ and 10 ng/mL for IL-1α after equilibration with the agarose gel. Medium was changed three times each week.

3D Ring Tissue Imaging

To quantify changes in time dependent tissue thickness, brightfield imaging was performed at days 2, 4, 7,and 14 using a PCO.panda 4.2 USB3.1 sCMOS camera (Nikon, Tokyo, Japan) and a 2x Objective **(Figure 4)** . Automated *(x,y)* thickness measurements were obtained

through a custom General Analysis 3 (GA3) workflow within NIS-Elements AR (v6.10.01). This automated protocol utilized light-intensity thresholding to define ring boundaries, supplemented by manual inclusionary and exclusionary tools. To provide confidence in measurements of the ring thickness, the GA3 module generated 1,000 equidistant measurements derived from 500 radial vectors originating from the sample's geometric center.

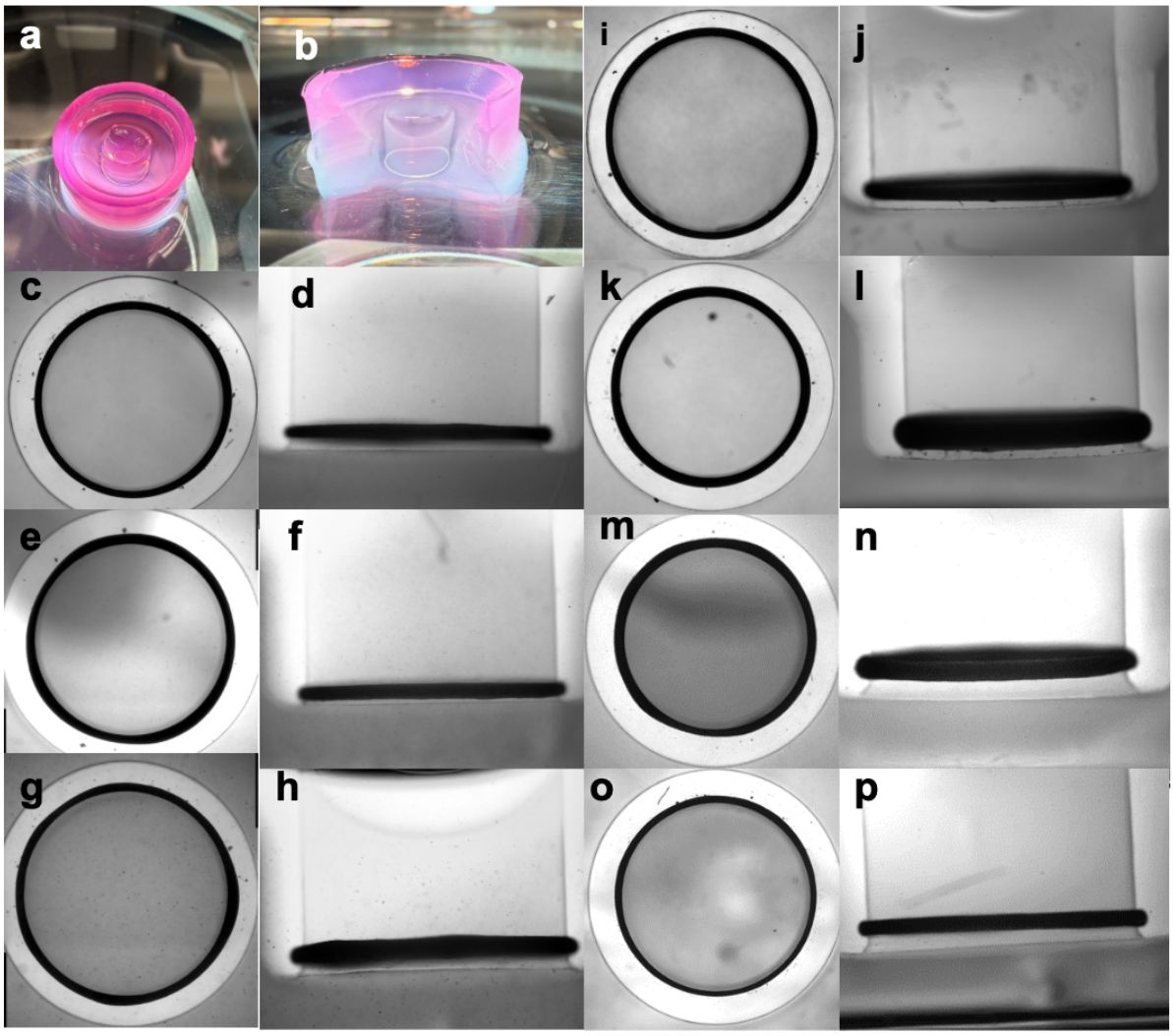

Figure 4. Formation of ring-shaped tissues in vitro. Photograph of a ring-shaped tissue (5mm inner diameter) in a molded agarose gel removed from a 24 well plate (a) and gel sliced to

reveal the ring-shaped tissue (b). Conventional (c, e, g, i, k,o) and side-view (d, f, h, j, l,p) brightfield images of a day 14 control untreated tissue (c, d) and day 14 tissues treated with TNF-α (e, f), IL-18 (g, h), IL-1β (i, j),TGF-β1 (k, l), IFN-γ (m,n) or IL-1α (o,p).

Raw data was compiled and standardized using a custom Python-based processing script. This automation consolidated individual sample measurements into a unified database, filtered for sampling outliers, and calculated the mean thickness and standard deviation for each tissue. Following the final timepoint at day 14, side-view images (z) were acquired by harvesting samples into a custom-designed cutting block (SolidWorks Corp., Concord, MA) **(Figure 5)**. The agarose gels were cut using a razor blade and imaged to visualize all 4 sides of the ring tissue. These 4 images were used to obtain 12 distinct thickness measurements across the *(z)* dimension of the ring. Final cross-sectional area (CSA) and total volume were then calculated by integrating the *(x,y)* thickness measurements with the *(z)* dimension measurements **(Figure 5)**.

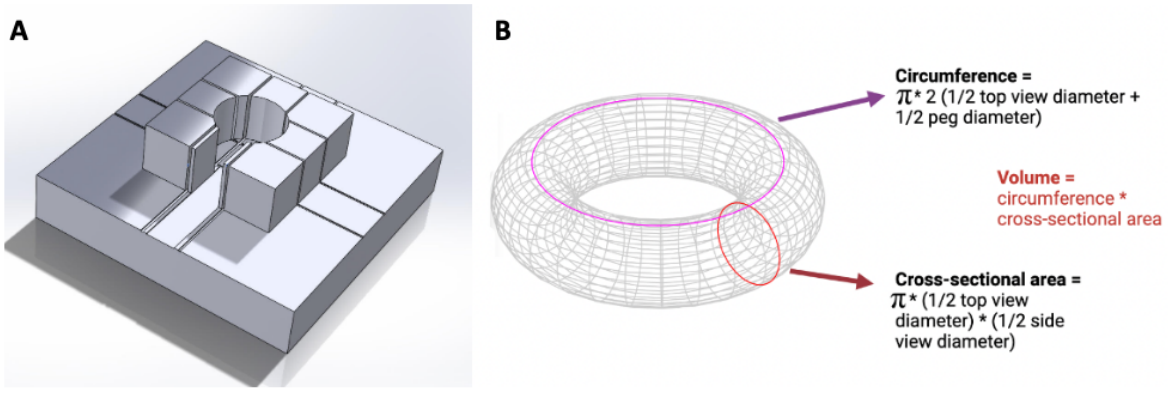

Figure 5: Chopping block for side-view gel imaging. A chopping block was designed in SolidWorks (Concord, MA) and 3D printed on a Form 3 printer (Formlabs, Inc., Somerville, MA). Gels containing ring tissue were removed from 24-well plates using a spatula, placed into the chopping block, and trimmed to four flat sides using a razor blade guided by the block's slots. The trimmed gel was then laid on its side in a tissue culture plate, and brightfield images of all four sides were acquired using an inverted microscope.

Tensile Testing of 3D Ring tissues

Mechanical testing of 3D ring microtissues were performed using an Instron tensile tester (Instron 5943, Norwood, MA) using a 5N load cell with a 5mN resolution. Fourteen day old ring tissues were first imaged for *(x,y)* and *(z)* followed by removal from the gel and placed on a custom 3D printed gripper made from glass-filled nylon (ProtoLabs, Maple Plan, MN) laying horizontally in a separate PBS bath. The custom gripper was composed of two pieces, with a half cylinder with a 1.5 mm radius and on both sides four securing pieces connecting the two bases together **(Figure 6)**. The bottom gripper was secured into a custom PBS bath attached to the lower Instron fixture and heated to 37 °C for 1 hour prior to testing. The top Instron fixture was then attached to the top gripper and the four securing pieces were removed. The distance between the two base pieces was extended to 2 mm to achieve a distance equivalent to 5 mm diameter. Tensile testing was done at a rate of 0.1% initial length/ second. While the testing was in progress the values of load (N) and extension (mm) were recorded by Bluehill Software by Instron. Automatic termination was set in place to terminate the sample once a load drops below 40% indicating sample failure. Rings were collected and stored at -80°C after mechanical testing for collagen and DNA measurements.

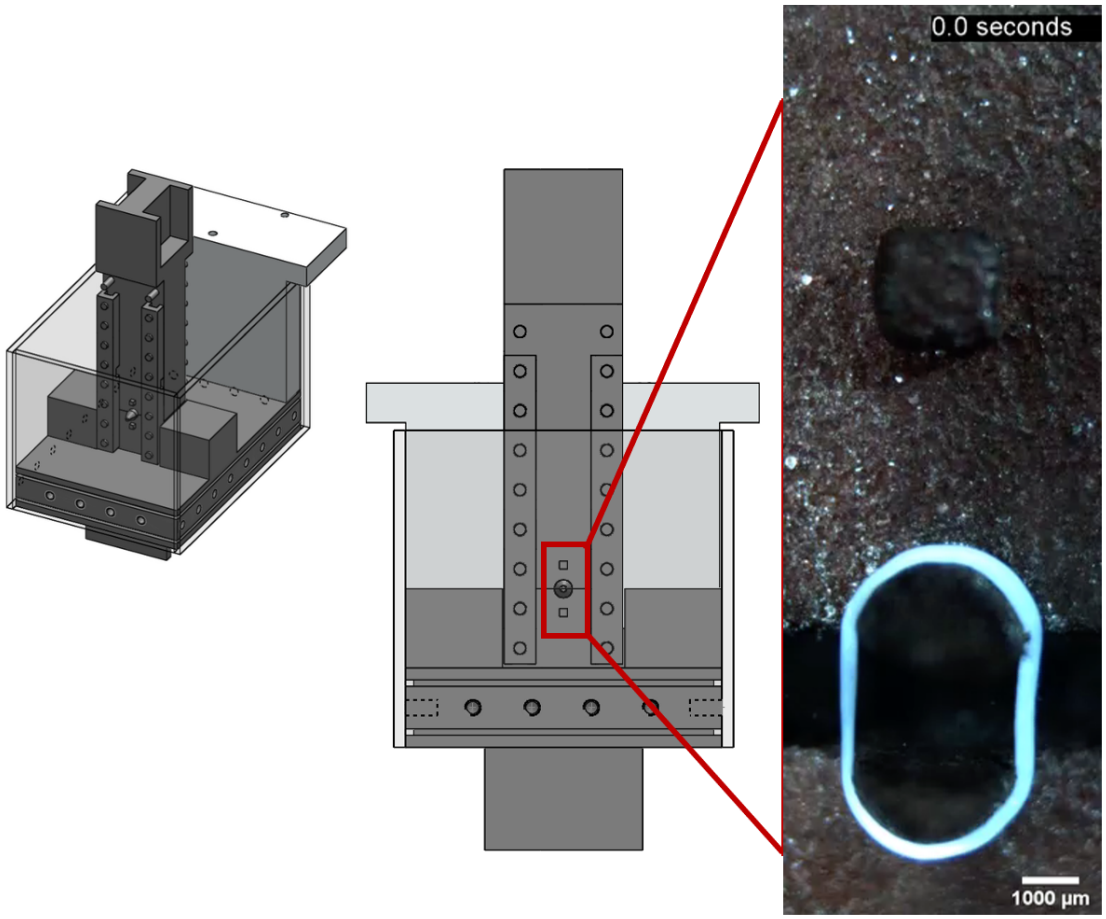

Figure 6: Custom Grippers for Tensile Testing of Ring tissues. SolidWorks files of the custom created grippers made from a top grip and bottom grip piece along with four securing strips to load and test 5 mm microtissue rings. Ring tissues tested on day 14. Wilks, B. T. et al. [9]

Molecular and Biochemical Assays

To quantify total collagen, rings were digested in 125 ug/mL papain (#P4762, Sigma Aldrich) at pH 6.5 at 65 °C for 10 days and levels of hydroxyproline measured using a colorimetric assay[10]. Digested tissues were diluted with an equal volume of 4M NaOH (#S318-1, Fisher), incubated at 120 °C for an hour and neutralized with an equal volume of 4M HCl (#SA56-1, Fisher). Chloramine T solution (#S318-1, Fisher) was added and samples incubated at

room temperature for 20 minutes. Ehrlich's reagent (#LC140802, LabChem) was added and samples incubated at 65°C for 30 minutes. Samples were transferred to a 96-well plate and absorbance at 550 nm read using a UV plate reader (SpectaMax Plus 384, Molecular Devices, San Jose, CA). Values of collagen (ug/ring) were calculated from a standard curve (Type I rat tail collagen #5056, Advanced Biomatrix, Carlsbad, CA).

Total DNA content was quantified using the Quant-iT PicoGreen dsDNA Assay Kit (#P11496, Invitrogen, Waltham, MA) per the manufacturer's protocol using the papain digested samples prepared for collagen analysis. Samples were incubated with the picogreen working solution at room temperature for 5 minutes, transferred to a 96- well plate and fluorescence (480 nm excitation, 520 nm emission) measured using a fluorescent plate reader (SpectraMax Gemini XS, Molecular Devices). Values of DNA (ng/mL) were derived from a standard curve of λ DNA ((#P11496, Invitrogen). Three to four technical replicates from three independent biological experiments were run for each condition for an *n* equal to ten.

Histology of Ring tissues

Ring tissues were fixed in 10% buffered formalin and kept at 4°C until prepared for embedding. For preparation of the embedding process, rings were kept on the peg and cut using a razor blade and custom 3D printed chopping block **(Figure 5)**. The cut agarose gel was transferred to a 24-well plate, and each well was filled with an additional 2% (w/v) agarose/PBS to encapsulate the original mold and secure the microtissue ring. Once the fresh agarose had gelled, the agarose puck was transferred to a cassette and paraffin embedded. Samples were cut into 5-10 μm sections using a Leica RM2265 microtome (Leica Microsystems, Wetzlar, Germany). Slides were stained with hematoxylin and eosin (Richard-Allan Scientific; Thermo

Scientific) or Masson's Trichrome (Electron Microscopy Sciences, Hatfield, PA) according to the manufacturer's protocols. All slides were viewed and digitized using an Olympus VS200 Slide Scanner (Olympus, Tokyo, Japan) with associated VS200 ASW software followed by viewing in OlyVIA (Olympus, open access).

Data Analysis and Statistical Analysis

All data were graphically and statistically analyzed using GraphPad Prism (GraphPad Software, San Diego, CA). For comparisons between two unpaired groups, Welch's t-test was applied to data following a Gaussian distribution, and the Mann–Whitney test was used for non-parametric data. Statistical significance is indicated by asterisks following the standard GraphPad settings ($p < 0.05$, $p < 0.01$, $p < 0.001$).

Results

TNF-α, IL-1β, IL-18, IFN-γ and IL-1α alter the thickness of control tissues

Twenty-four hours after cell seeding, rings were treated with either TNF-α (10 ng/ml), IL-18 (50 ng/ml), IL-1β (50 ng/ml), IFN-γ (5 ug/mL) or IL-1α (10 ng/mL). Untreated rings served as the control with the vehicle for each of the respective cytokines. To quantify changes to tissue thickness, the dimensions of tissues treated with either TNF-α, IL-18, IL-1β, IFN-γ or IL-1α were measured and compared to untreated control rings **(Figure 7)**. TNF-α increased the *(x,y)* thickness of day 7 tissues, but interestingly TNF-α decreased the *(x,y)* thickness of day 14 tissues. IL-18 and IFN-γ increased in *(x,y)* thickness at days 7 and 14. Whereas, IL-1β and IL-1α treated rings decreased in *(x,y)* thickness at days 7 and 14. On day 14, measurements of the *(z)* thickness were also taken. TNF-α and IL-1β decreased *(z)* thickness, while IL-18 increased *(z)* thickness. IL-1α and IFN-γ were not significantly different in the *(z)* dimension on day 14.

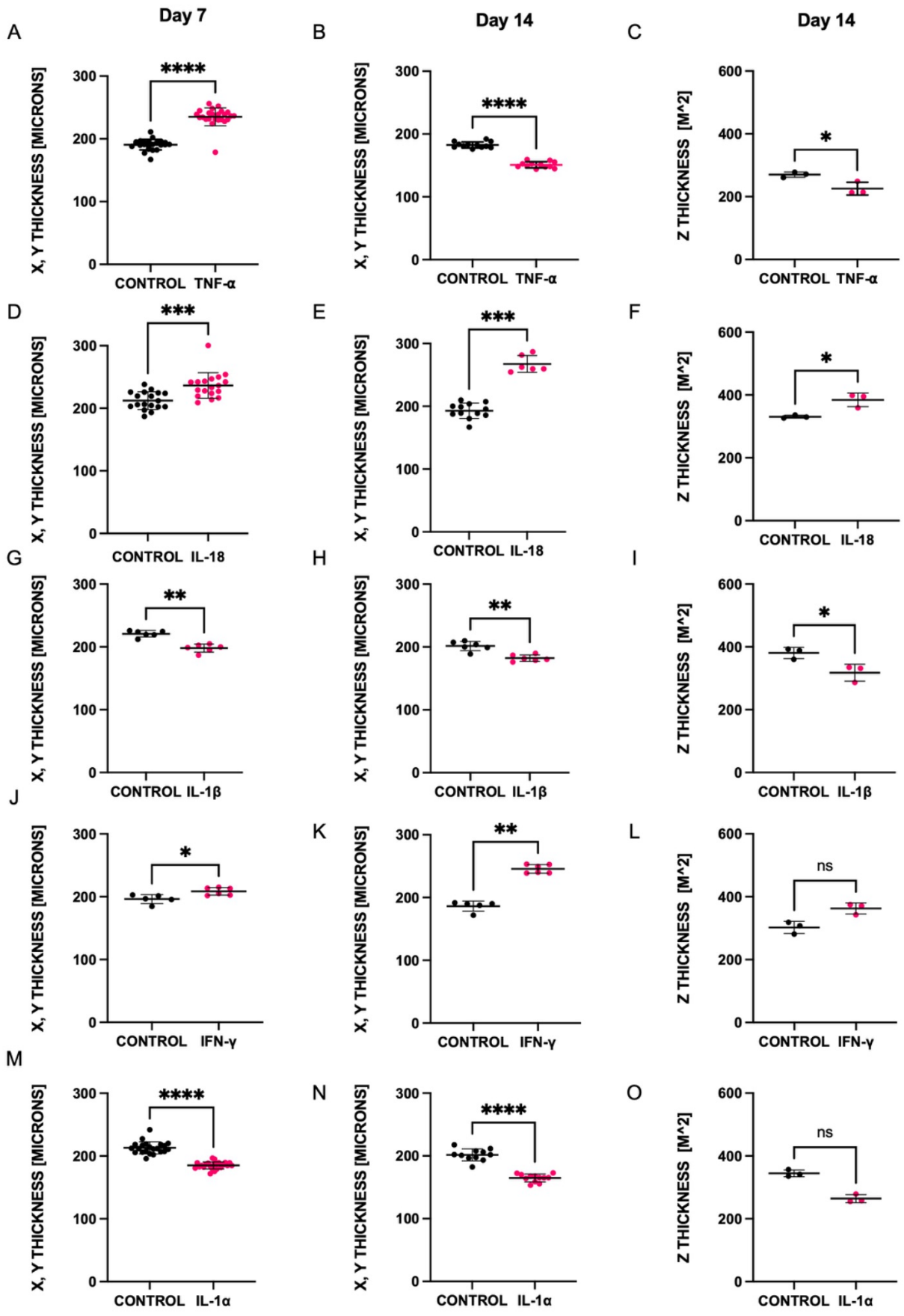
Day 7
Day 14
Day 14
A
B
C
D
E
F
G
H
I
J
K
L
M
N
O
X, Y THICKNESS [MICRONS]
Z THICKNESS [M^2]
CONTROL TNF-α
CONTROL IL-18
CONTROL IL-1β
CONTROL IFN-γ
CONTROL IL-1α
****
***
**
*
ns
0
100
200
300
400
600

Figure 7: TNF-α , IL-1β , and IL-1α but not IL-18 or IFN-γ , decrease the size of control tissues. Measurements of the x, y dimensions (a, b, d, e, g, h, j, k ,m, n) and z dimensions (c, f, i, l, o) of tissues at day 7 (a, d, g, j, m) and day 14 (b, e, h, k, n). Control untreated tissues are compared to tissues treated with TNF-α, IL-18, IL-1β, IFN-γ, or IL-1α (a-o).

The thickness of TGF-β1 stimulated tissues is decreased by TNF-α, IL-1β and IL-1α.

TGF-β1 is widely recognized as a major driver of fibrosis and previously we've demonstrated that TGF-β1 increases size, total collagen, and tensile properties of ring tissues [9]. To determine if addition of a second cytokine could alter the TGF-β1 response, tissues were treated with TGF-β1 (10 ng/ml) plus either TNF-α, IL-18, IL-1β, IFN-γ or IL-1α . To determine cytokine influence on the TGF-β1-mediated increase in thickness, the dimensions of TGF-β1 treated tissues were compared to tissues treated with TGF-β1 plus TNF-α, TGF-β1 plus IL-18, TGF-β1 plus IL-1β, TGF-β1 plus IFN-γ or TGF-β1 plus IL-1α **(Figure 8)**. Acting alone, TNF-α increased the thickness of control tissues, but when combined with TGF-β1, TNF-α was neither neutral nor synergistic with the TGF-β1 mediated increase in thickness. The combination of TNF-α and TGF-β1 caused a significant decrease in thickness at day 7 as well as day 14 compared to tissues treated with TGF-β1 alone. The combination of IL-18 and TGF-β1 increased thickness at day 7, but not day 14. In contrast, tissues treated with a combination of IL-1β plus TGF-β1 and IL-1α plus TGF-β1 decreased in thickness at days 7 and 14. The combination of IFN-γ and TGF-β1 increased the thickness of ring tissues at both day 7 and 14.

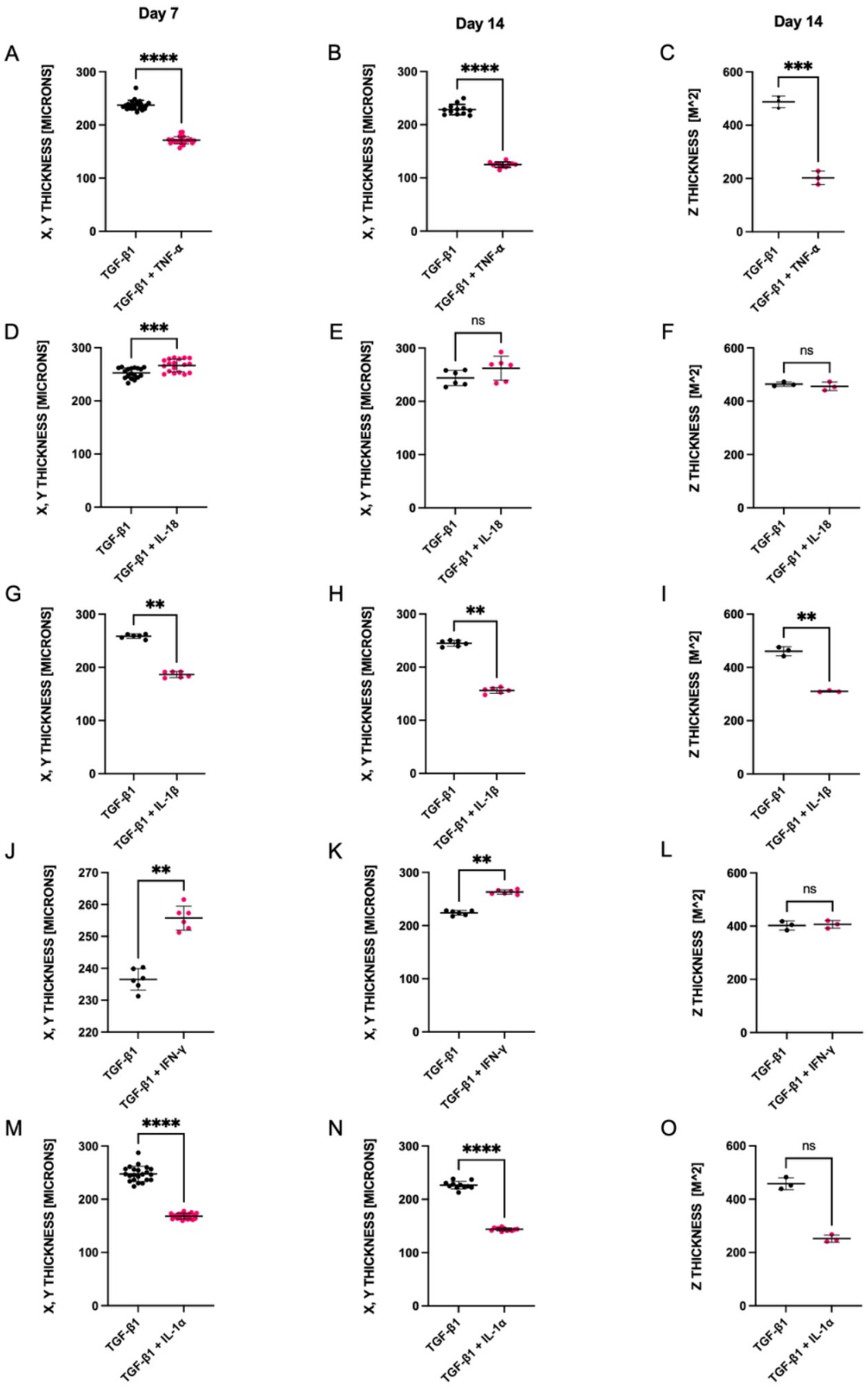
Day 7
Day 14
Day 14
A
B
C
D
E
F
G
H
I
J
K
L
M
N
O
X, Y THICKNESS [MICRONS]
Z THICKNESS [M^2]
****
***
**
ns
TGF-β1
TGF-β1 + TNF-α
TGF-β1 + IL-18
TGF-β1 + IL-1β
TGF-β1 + IFN-γ
TGF-β1 + IL-1α

Figure 8: TNF-α, IL-1β and IL-1α, but not IL-18 or IFN-γ, decrease the size of TGF-β1 treated tissues. Measurements of the x, y dimensions (a, b, d, e, g, h, j, k, m, n) and z dimensions (c, f, i, l, o) of tissues at day 7 (a, d, g, j, m) and day 14 (b, e, h, k, n). Tissues treated with TGF-β1 are compared to tissues treated with TGF-β1 plus TNF-α, TGF-β1 plus IL-18, TGF-β1 plus IL-1β, TGF-β1 plus IFN-γ or TGF-β1 plus IL-1α (a-o).

Differential effects of TNF-α, IL-1β, IL-18, IFN-γ and IL-1α on total DNA of control and TGF-β1 stimulated tissues

To determine if cytokine treatment altered total DNA, tissues harvested at days 7 and 14 were digested in papain and the amount of DNA measured using a fluorescent assay **(Figure 9)**. TNF-α had no effect on total DNA of control tissues at days 7 or 14 but decreased total DNA of TGF-β1 stimulated tissues at days 7 and 14. In contrast, IL-18 increased total DNA of control tissues at days 7 and 14 but had no effect on TGF-β1 stimulated tissues. IL-1β and IFN-γ had no effect on total DNA at day 7 of control or TGF-β1 stimulated tissues. At day 14, IL-1β increased total DNA of control tissues, but decreased total DNA of TGF-β1 stimulated tissues. IFN-γ at day 14 increased total DNA content compared to both control and TGF-β1 stimulated tissues. At day 7, IL-1α decreased DNA in both control and TGF-β1 stimulated tissues. At day 14, IL-1α was not significantly different from control but was decreased when compared to TGF-β1 stimulated tissues.

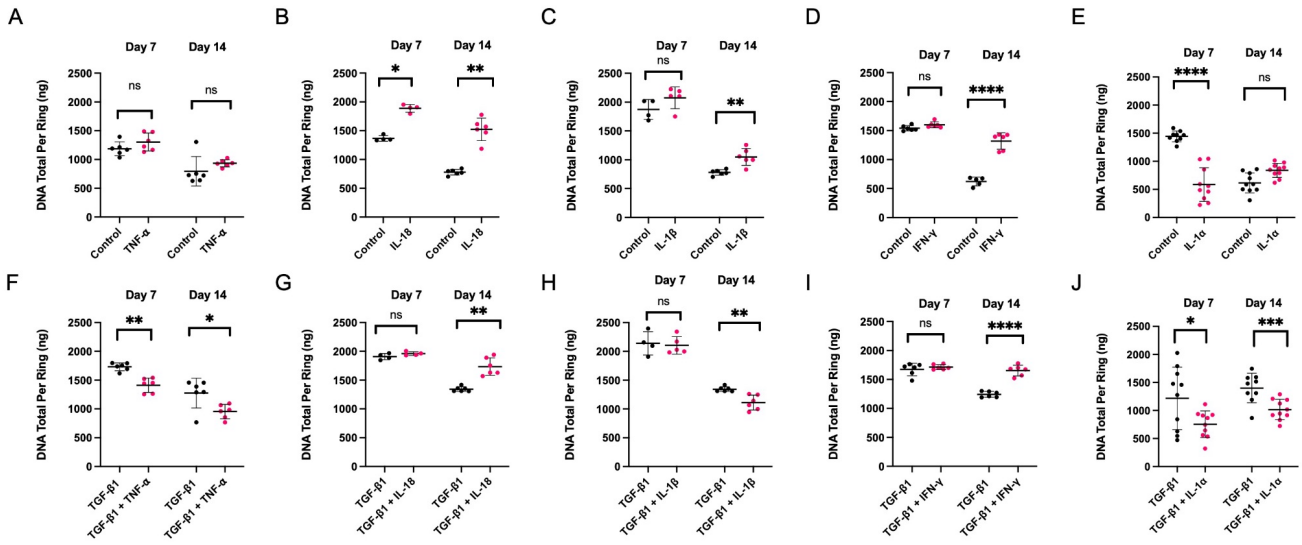

Figure 9. Effects of TNF-α, IL-1β, IL-18, IFN-γ and IL-1α on total DNA of control and TGF-β1 stimulated tissues. Measurements of total DNA content of tissues at days 7 and 14 treated with TNF-α (a), IL-18(b), IL-1β (c), IFN-γ (d), IL-1α (e), TGF-β1 plus TNF-α (f), TGF-β1 plus IL-18 (g), TGF-β1 plus IL-1β (h), TGF-β1 plus IFN-γ (i) or TGF-β1 plus IL-1α (j).

TNF-α, IL-1β and IL-1α, but not IL-18 or IFN-γ, reduce total collagen of control or TGF-β1 stimulated tissues

To determine if cytokine treatment altered total collagen, tissues harvested at days 7 and 14 were digested in papain and the amount of hydroxyproline measured using a colorimetric assay **(Figure 10)**. TNF-α and IL-1α decreased total collagen of control tissues at days 7 and 14. The decrease in collagen was even greater for TGF-β1 stimulated tissues for both of these conditions. In contrast, IL-18 had no effect on total collagen of control or TGF-β1 stimulated tissues at days 7 or 14. IL-1β decreased total collagen of control tissues at days 7 and 14. Like TNF-α's action, the IL-1β mediated decrease of total collagen was even greater when combined with TGF-β1 at

days 7 and 14. At days 7 and 14, IFN-γ was not significantly different when compared to control or TGF-β1 stimulated tissues.

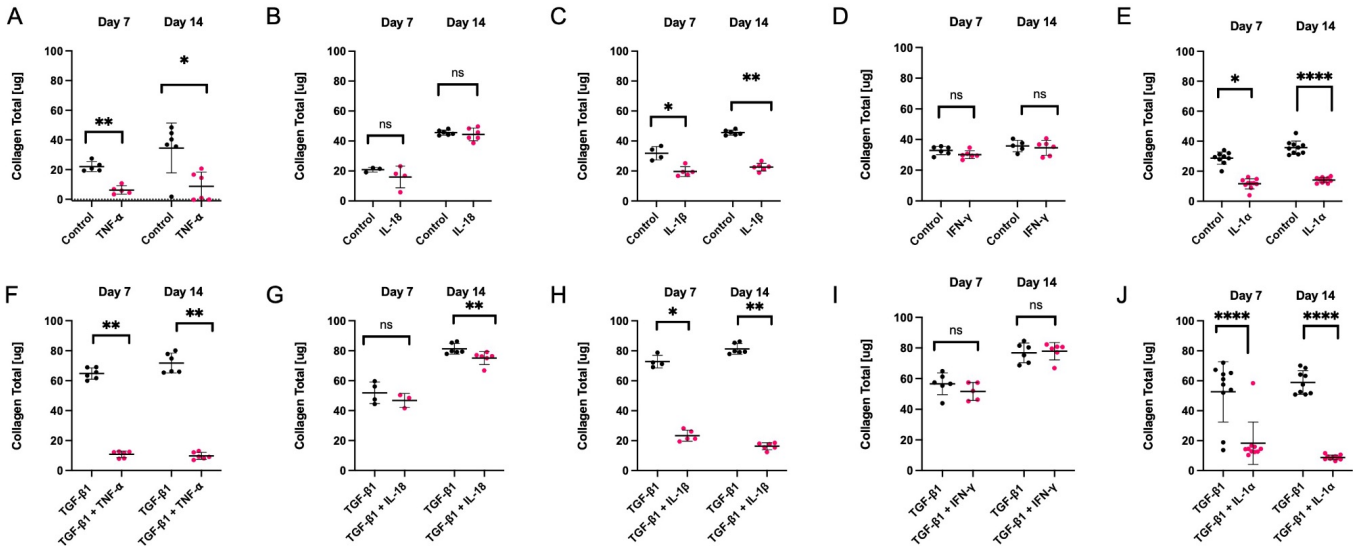

Figure 10. TNF-α, IL-1β and IL-1α, but not IL-18 or IFN-γ, reduce total collagen of control and TGF-β1 stimulated tissues. At day 7 and day 14 tensile tested tissues were frozen, solubilized by papain digestion and levels of hydroxyproline assayed to measure total collagen. Control untreated tissues are compared to tissues treated with TNF-α, IL-18, IL-1β, IFN-γ or IL-1α (a, b, c, d, e). Tissues treated with TGF-β1 are compared to tissues treated with TGF-β1 plus TNF-α, TGF-β1 plus IL-18, TGF-β1 plus IL-1β, TGF-β1 plus IFN-γ or TGF-β1 plus IL-1α (f, g, h, i, j).

TNF-α and IFN-γ, but not IL-1β, IL-18 or IL-1α, reduce the strength and stiffness of control tissues

To determine if cytokine treatment altered the biomechanics of the ECM, tissues at day 14 were removed from the gels and subjected to tensile testing to measure ultimate tensile strength (UTS, strength) and maximum tangent modulus (MTM, stiffness) **(Figure 11)**. All values were normalized to the cross-sectional area (CSA) of each tissue as calculated from their respective *x, y* and *z* measurements. TNF-α (a, f) and IFN-γ (d, i) decreased the strength and stiffness of control. In contrast, IL-1β (b, g), IL-18 (c, h) and IL-1α had no effect on the strength or stiffness of control tissues.

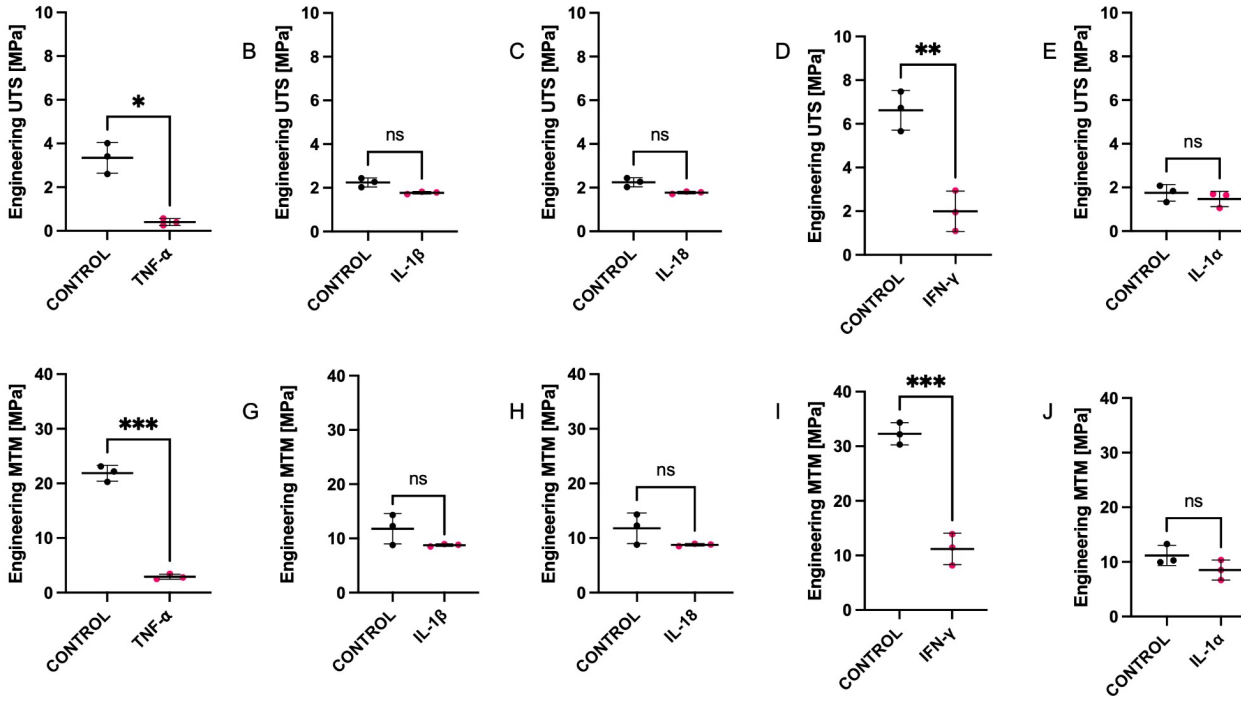

Figure 11. TNF-α and IFN-γ, but not IL-18, IL-1β, or IL-1α, reduce strength and stiffness of control-stimulated tissues. At day 14 (a-j), tissues were removed from the gel and tensile tested

to measure ultimate tensile strength (UTS, strength) (a-e) and maximum tangent modulus (MTM, stiffness) (f-j). Control untreated tissues are compared to tissues treated with TNF-α, IL-18, IL-1β, IFN-γ or IL-1α.

TNF-α, IL-1β, IL-1α but not IL-18 or IFN-γ, reduce the strength and stiffness of TGF-β1 stimulated tissues

All values were normalized to the cross-sectional area (CSA) of each tissue as calculated from their respective *x, y* and *z* measurements. All conditions were also tested in the presence of TGF-β1 **(Figure 12)**. TGF-β1 historically in the 3D ring tissue system increases both MTM and UTS compared to untreated control tissues. TNF-α plus TGF-β1, IL-1β plus TGF-β1 and IL-1α plus TGF-β1 decreased the strength and stiffness of TGF-β1 stimulated tissues. In contrast, IL-18 plus TGF-β1 and IFN-γ plus TGF-β1had no effect on the strength or stiffness of TGF-β1 stimulated tissues.

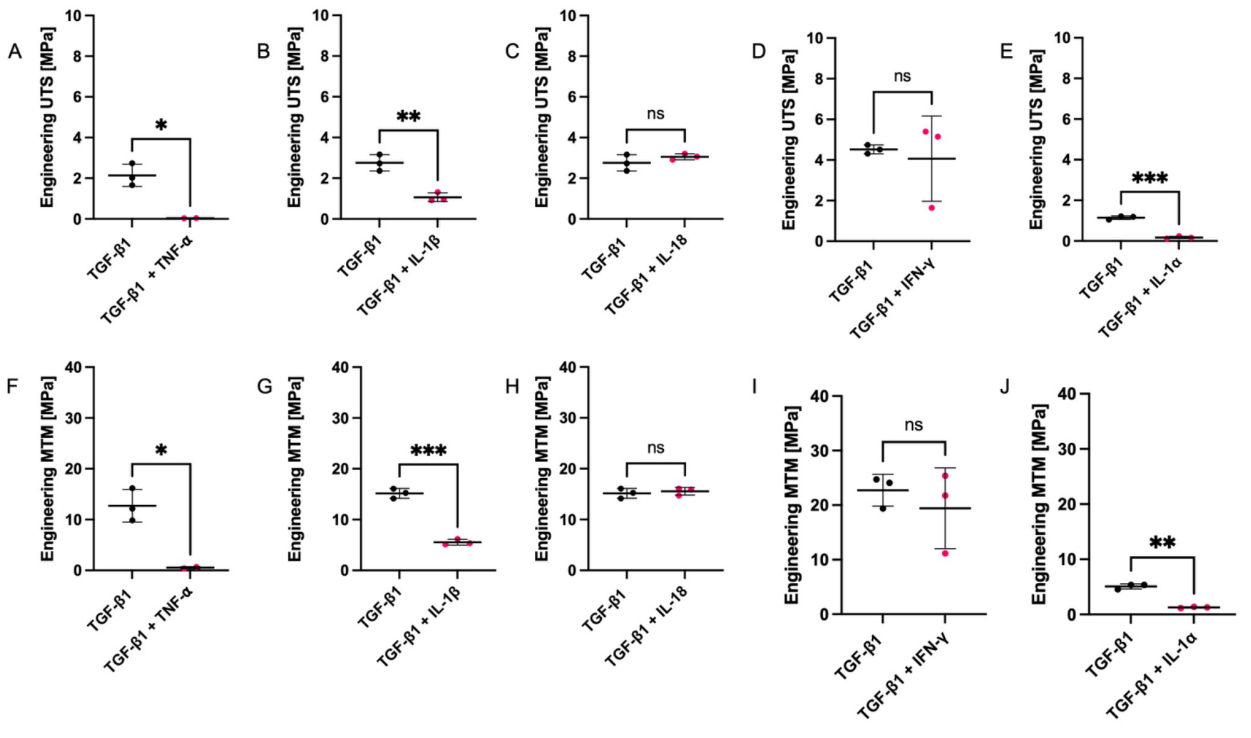

Figure 12. TNF-α, IL-1β, IL-1α but not IL-18 or IFN-γ, reduce strength and stiffness of TGF-β1 stimulated tissues. At day 14 (a-j), tissues were removed from the gel and tensile tested to measure ultimate tensile strength (UTS, strength) (a-e) and maximum tangent modulus (MTM, stiffness) (f-j). Tissues treated with TGF-β1 are compared to tissues treated with TGF-β1 plus TNF-α, TGF-β1 plus IL-18, TGF-β1 plus IL-1β, TGF-β1 plus IFN-γ, or TGF-β1 plus IL-1α.

TNF-α and IL-1β, but not IL-18, alter the histology of ring-shaped tissues

At day 7 and day 14, tissues were formalin fixed and paraffin embedded, and sections were stained with hematoxylin and eosin (H&E) **(Figures 13, 14)** or Masson's Trichrome **(Figures 15, 16)**. H&E and trichrome images were reviewed at day 7 and day 14 across multiple fields per slide, with attention to reproducible areas and consistent focus. Control untreated tissues matured as expected between day 7 and day 14, with decreased tissue thickness, stronger trichrome staining, and progressive organization of collagen into parallel bundles **(Figures 13, 15)**. TGF-β1 treated tissues followed a similar trajectory, with collagen deposition at least comparable to untreated controls and more clearly aligned fiber architecture by day 14 **(Figures 14, 16)**. IL-18 treated tissues were broadly similar to control at both timepoints, showing no consistent difference in collagen amount or fiber organization **(Figures 13, 15)**.

In contrast, tissues treated with TNF-α or IL-1β showed a looser, less organized matrix at both timepoints **(Figures 13, 15)**. This effect was most pronounced at day 14 in the combination groups, where TGF-β1 plus TNF-α and TGF-β1 plus IL-1β tissues showed reduced trichrome intensity across many fields and a shift away from parallel fiber alignment toward a whorled or interlacing pattern **(Figures 14, 16)**. H&E staining of these tissues revealed increased nuclear density with shrunken, darkly stained nuclei consistent with pyknosis **(Figures 13, 14)**. Small eosinophilic areas with low nuclear density were occasionally observed in these groups, though they were rare and focal. These histological findings are consistent with the biochemical and biomechanical data, with the most pronounced changes in collagen architecture and nuclear morphology occurring in the TNF-α and IL-1β conditions, particularly in combination with TGF-β1, and the clearest separation between groups evident at day 14.

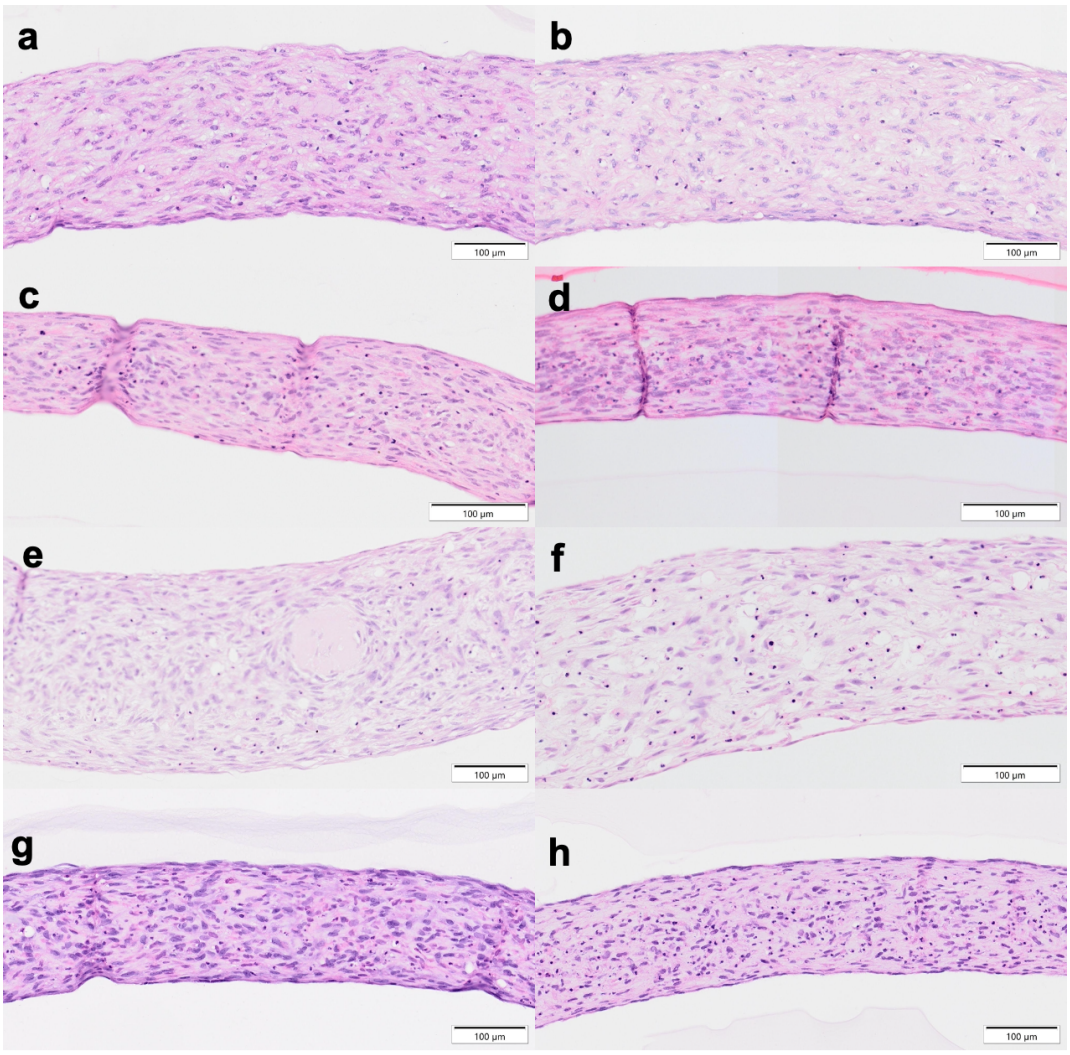

Figure 13. TNF-α and IL-1β, but not IL-18, alter tissue histology. At day 7 (a, c, e, g) and day 14 (b, d, f, h), tissues were formalin fixed, paraffin embedded, and sections stained with hematoxylin and eosin (H&E). Shown are control untreated tissues (A, B) and tissues treated with TNF-α (c, d), IL-18 (e, f) or IL-1β (g, h). Scale bar = 100 um.

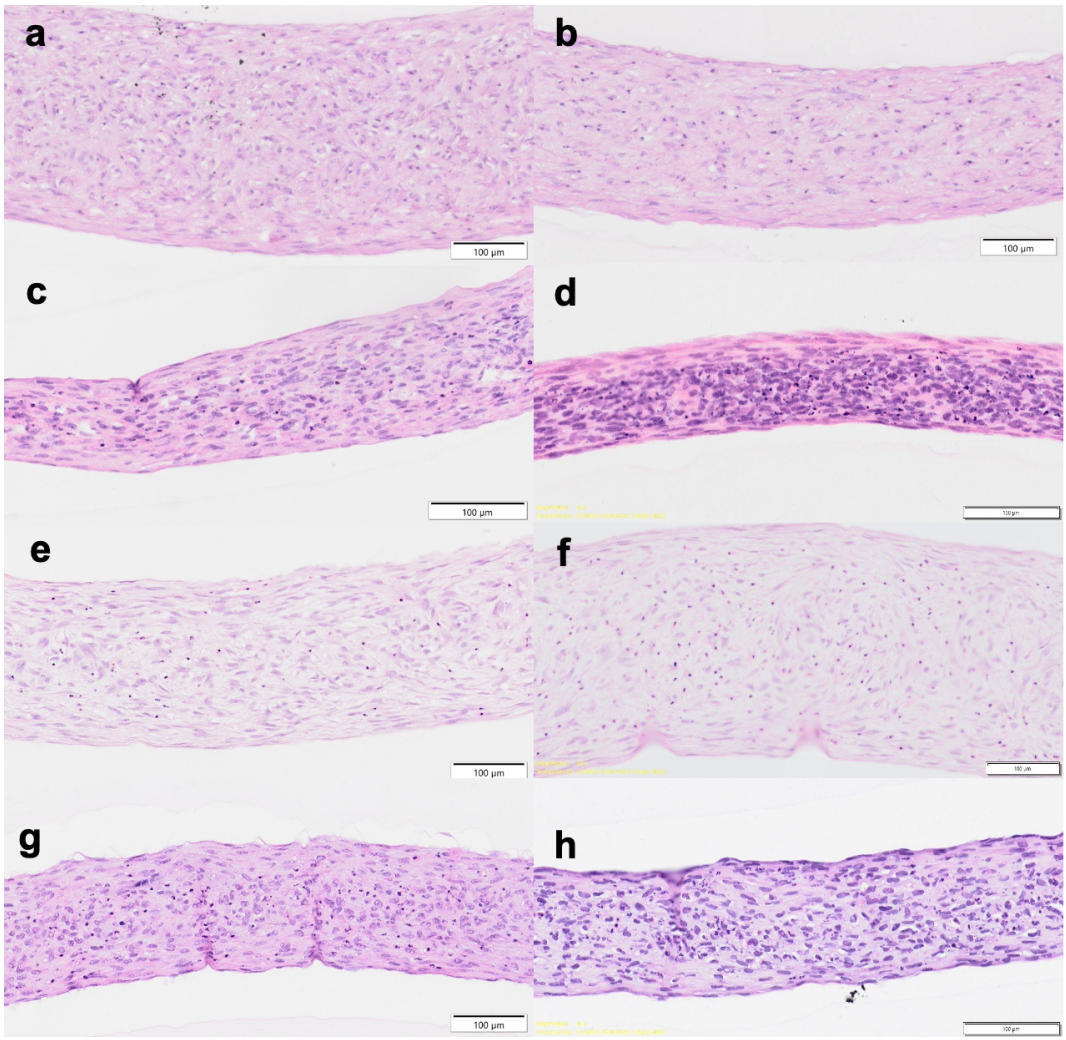

Figure 14. TNF-α and IL-1β, but not IL-18, alter the histology of TGF-β1 stimulated tissues. At day 7 (a, c, e, g) and day 14 (b, d, f, h), tissues were formalin fixed, paraffin embedded, and sections stained with hematoxylin and eosin (H&E). Shown are tissues treated with TGF-β1 alone (a, b) and tissues treated with TGF-β1 plus TNF-α (c, d), TGF-β1 plus IL-18 (e, f), or TGF-β1 plus IL-1β (g, h). Scale bar= 100 um.

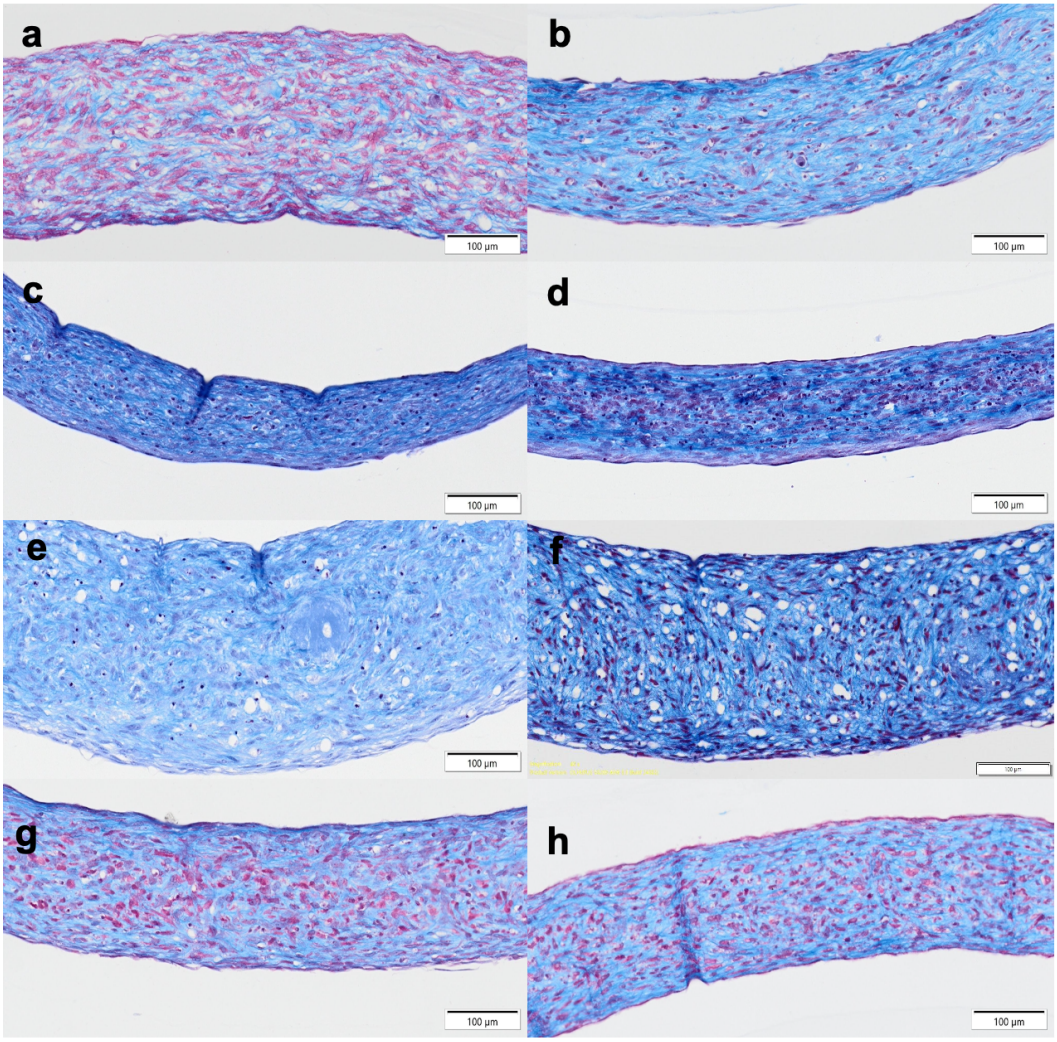

Figure 15. TGF-β1, TNF-α and IL-1β, but not IL-18, alter tissue histology. At day 7 (a, c, e, g) and day 14 (b, d, f, h), tissues were formalin fixed, paraffin embedded, and sections stained with Masson's Trichrome. Shown are control untreated tissues (a, b) and tissues treated with TNF-α (c, d), IL-18 (e, f) or IL-1β (g, h). Scale bar = 100 um.

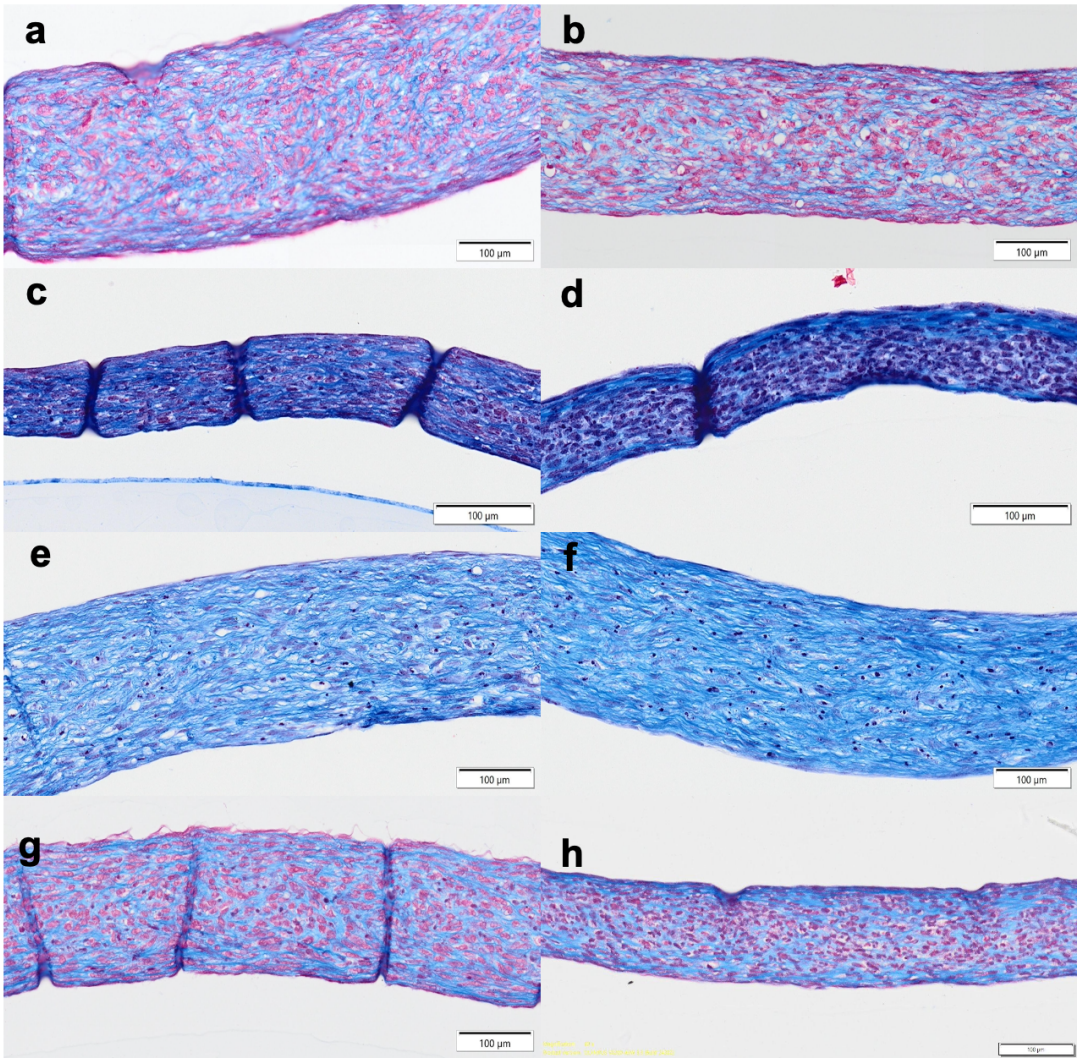

Figure 16. TNF-α and IL-1β, but not IL-18, alter the histology of TGF-β1 stimulated tissues. At day 7 (a, c, e, g) and day 14 (b, d, f, h), tissues were formalin fixed, paraffin embedded, and sections stained with Masson's Trichrome. Shown are tissues treated with TGF-β1 alone (a, b) and tissues treated with TGF-β1 plus TNF-α (c, d), TGF-β1 plus IL-18 (e, f), or TGF-β1 plus IL-1β (g, h). Scale bar = 100 um.

To summarize the effects of each cytokine on tissue size, collagen content, DNA, and biomechanical properties, the data from day 7 and 14 are compiled **(Table 1)**. Each cytokine is shown both alone and in combination with TGF-β1, with arrows indicating the direction of change relative to the appropriate control. These summary patterns demonstrate that while TNF-α, IL-1β, and IL-1α consistently counteract TGF-β1-driven collagen accumulation and mechanical properties, IL-18 and IFN-γ remain largely neutral across most parameters.

	Cytokine Alone							Cytokine combined with TGF-β1					
	X,Y	**Z**	**UTS**	**MTM**	**COL**	**DNA**		**XY**	**Z**	**UTS**	**MTM**	**COL**	**DNA**
Day 7 TNF-α	↑				↓	**ns**		↓				↓	↓
Day 14 TNF-α	↓	↓	↓	↓	↓	**ns**		↓	↓	↓	↓	↓	↓
Day 7 IL-18	↑					↑		↑				**ns**	**ns**
Day 14 IL-18	↑	↑	**ns**	**ns**	**ns**	↑		**ns**	**ns**	**ns**	**ns**	**ns**	**ns**
Day 7 IL-1β	↓					**ns**		↓				↓	**ns**
Day 14 IL-1β	↓	↓	**ns**	**ns**	↓	↑		↓	↓	↓	↓	↓	↓
Day 7 IFN-γ	↑				**ns**	**ns**		↑				**ns**	**ns**
Day 14 IFN-γ	↑	**ns**	↓	↓	**ns**	↑		↑	**ns**	**ns**	**ns**	**ns**	↑
Day 7 IL-1α	↓				↓	↓		↓				↓	↓

Day 14 IL- 1α	↓	**ns**	**ns**	**ns**	↓	**ns**		↓	**ns**	↓	↓	↓	↓

Table 1: Summary of the thickness, biochemical and mechanical effects of proinflammatory cytokines on control and TGF-β1-stimulated 3D ring tissues. The impact of each cytokine on thickness (X,Y and Z), Ultimate Tensile Strength (UTS), Maximum Tangent Modulus (MTM), total collagen and total DNA is shown relative to untreated controls or TGF-β1-only treated tissues. Red cells with an upward arrow (↑) indicate a significant increase, green cells with a downward arrow (↓) indicate a significant decrease, and grey cells (ns) indicate no significant change.

Discussion and Conclusion

The inflammatory environment present in fibrotic tissue is composed of a diverse array of cytokines that signal both immune cells and fibroblasts[4,5,6]. While TGF-β1 is widely recognized as the primary driver of fibrosis, other proinflammatory cytokines are present in the fibrotic niche and may act on fibroblasts to modulate TGF-β1's effects. How fibroblasts integrate and respond to these signals collectively is not well understood. In this study, we used a long-term 3D *in vitro* model of collagen-rich human connective tissue to investigate the individual and combined effects of five proinflammatory cytokines: TNF-α, IL-1β, IL-1α, IL-18, and IFN-γ, both alone and in combination with TGF-β1. Despite their pro-inflammatory nature, none of the cytokines increased collagen accumulation beyond basal levels, either alone or when combined with TGF-β1.

These cytokines and TGF-β1 are expressed by both fibroblasts and immune cells during fibrosis [4,5,6]. Because fibroblasts both secrete and respond to these cytokines, autocrine and paracrine signaling are likely occurring simultaneously in the fibrotic environment. This expression is context-dependent and is triggered by tissue injury, mechanical stress, and immune cell activation. Each cytokine's release is also tightly regulated. TGF-β1 is stored as an inactive pro-form in the ECM and requires proteolytic activation before it can signal[12,13]. Similarly, IL-1β

and IL-18 are synthesized as inactive cytoplasmic precursors that depend on inflammasome activation for processing and release[26-29]. IL-1α, in contrast, does not require inflammasome processing and is instead released rapidly from damaged or necrotic cells as an alarmin[22]. TNF-α is expressed as a membrane-bound precursor and is shed in soluble form only following proteolytic cleavage[30-32]. In contrast, IFN-γ is primarily regulated at the transcriptional level and is secreted by activated T cells and natural killer cells in response to IL-12 and IL-18 signaling[22]. These distinct regulatory pathways ensure that each cytokine, including the neutral effect of IFN-γ, is available only under specific inflammatory conditions. These differences in regulation mean that each cytokine enters the fibrotic environment at distinct times and in response to distinct triggers.

TNF-α, IL-1β, and IL-1α each reduced tissue size, total collagen, and the tensile strength and stiffness of control ring tissues. When combined with TGF-β1, each of these cytokines also blunted the TGF-β1-mediated increases in collagen, strength, and stiffness. Thus, TNF-α, IL-1β, and IL-1α act as counter-regulators of TGF-β1-driven ECM remodeling in this model. Histological analysis of TNF-α and IL-1β treated tissues revealed a looser, less aligned collagen matrix and increased nuclear pyknosis, effects that were most pronounced in TGF-β1-stimulated tissues. These morphological changes are consistent with the biochemical and biomechanical data and suggest that reduced collagen content alone does not fully account for the loss of mechanical integrity. Disorganization of the matrix architecture likely also contributes.

Although TNF-α, IL-1β, and IL-1α share the ability to suppress ECM accumulation and counteract TGF-β1, their mechanisms of action differ. TNF-α signals through TNFR1 and TNFR2, while both IL-1β and IL-1α signal through the IL-1 receptor (IL-1R1) [26-30]. Despite these distinct receptor systems, all three cytokines converge on NF-κB and MAPK signaling, which likely contributes to their shared suppression of collagen synthesis and promotion of matrix degradation.

The close functional parallel between IL-1β and IL-1α is notable given that IL-1α is released as an alarmin in the early stages of tissue damage, whereas IL-1β appears later following inflammasome activation. These data suggest that regardless of when during the inflammatory response each cytokine is released, their effects on fibroblast-mediated ECM remodeling are similar. This has implications for how the early versus late inflammatory environment shapes the fibrotic tissue.

In contrast, IL-18 and IFN-γ had little to no measurable effect on collagen accumulation or ECM biomechanics of either control or TGF-β1 stimulated tissues. Although IL-18 is also an inflammasome-processed cytokine like IL-1β, it signals through a distinct receptor complex and its primary biological role appears to be the activation of NK cells and T cells rather than direct modulation of fibroblast matrix production[26,28]. The lack of effect on collagen or mechanics here supports the idea that IL-18's contribution to fibrosis may be indirect, acting on immune cells that in turn signal fibroblasts, rather than through direct fibroblast activation. IFN-γ is well-established as a suppressor of fibrotic signaling in 2D models, where it induces Smad7 and inhibits TGF-β1 signaling[21]. Its lack of effect on collagen accumulation in this 3D model suggests that fibroblasts embedded within a maturing collagen-rich tissue may respond differently to IFN-γ than fibroblasts cultured on plastic. Notably, IFN-γ did reduce the strength and stiffness of control tissues, suggesting some effect on matrix organization or crosslinking, even without a detectable change in total collagen. Together, these data suggest that both IL-18 and IFN-γ may play a more important role as paracrine signals to immune cells in the fibrotic environment than as direct modulators of fibroblast ECM production.

Receptor-mediated signaling of TNF-α, IL-1β, IL-1α, and IL-18 all converge on the canonical NF-κB and MAPK pathways[26-32]. TGF-β1 signals through its own receptor and the canonical TGF-β/Smad pathway[12,13,33]. Given that TNF-α, IL-1β, and IL-1α all suppress TGF-β1-

mediated ECM remodeling while IL-18, which activates the same canonical NF-κB and MAPK pathways, does not, the differential outcomes are unlikely to be explained by canonical signaling alone. Rather, they are likely due to non-canonical signaling and context-dependent interactions with the activated TGF-β/Smad pathway that have yet to be fully defined. This model may be a useful tool for dissecting these pathway interactions.

Previously, this model was used to investigate the effects of IL-13, a proinflammatory cytokine that signals through the JAK/STAT pathway[11]. IL-13 alone had little effect on collagen or tissue mechanics, but when combined with TGF-β1, IL-13 produced increases in collagen, strength, and stiffness beyond what TGF-β1 alone could sustain over three weeks. Unlike the cytokines studied here, IL-13 is a paracrine cytokine produced exclusively by immune cells such as macrophages, eosinophils, and Th2 cells. These data suggest that TGF-β1-activated fibroblasts may require a paracrine immune cell signal to sustain long-term increases in collagen and mechanical properties. It would be interesting to test other immune-cell-exclusive cytokines, such as IL-4 and IL-17, both alone and in combination with TGF-β1. Conversely, it would be interesting to test anti-inflammatory paracrine cytokines such as IL-27, which is also expressed by immune cells in the fibrotic environment[4,5,7].

Most *in vitro* cytokine studies are performed on fibroblasts cultured as 2D monolayers for 24–48 hours[34-36]. In this model, cytokine effects are assessed on a 3D tissue over up to four weeks [9]. The data here suggest that fibroblast responses to cytokines are time dependent. The effects of TNF-α, IL-1β, and IL-1α on collagen production were evident by day 7 in both control and TGF-β1-stimulated tissues. TGF-β1 alone was similarly fast-acting, with effects evident at or before day 7 (data not shown). In contrast, the effects of IL-13 on TGF-β1-activated tissues required 2–3 weeks of exposure to manifest[11]. This suggests that cytokines in the fibrotic environment may

operate on distinct timescales, with TNF-α, IL-1β, IL-1α, and TGF-β1 acting as acute fast-responding signals, and cytokines like IL-13 acting as chronic signals that require prolonged exposure to produce measurable changes in ECM.

The cross-talk between autocrine and paracrine cytokines that drives fibrosis is complex and regulated at multiple levels. Using a 3D model of collagen-rich connective tissue, this study defines the roles of TNF-α, IL-1β, IL-1α, IL-18, and IFN-γ on control tissues and tissues activated with TGF-β1. Unexpectedly, TNF-α, IL-1β, and IL-1α each reduced tissue size, collagen content, and the strength and stiffness of both control and TGF-β1-stimulated tissues and altered tissue histology. In contrast, IL-18 and IFN-γ had little effect on collagen or tissue mechanics in either condition. This data demonstrate the complexity of proinflammatory cytokine signaling in the context of collagen accumulation and deposition , with TNF-α, IL-1β, and IL-1α acting as counter-regulators of TGF-β1-driven fibrosis, and IL-18 and IFN-γ playing a largely neutral role on fibroblasts directly. Stable for at least four weeks, this model can be used to define the effects of dose, exposure time, and cytokine combinations on ECM remodeling, and can be applied to fibroblasts from other organ systems. It may also be useful for identifying which cytokines drive the formation of the fibroblast subtypes identified in fibrotic tissues *in vivo* by single cell RNA sequencing [37–44].

References

1. Rockey, D. C., Bell, P. D. & Hill, J. A. Fibrosis--A Common Pathway to Organ Injury and Failure. N Engl J Med 373, 96 (2015).
2. Zhao, M. et al. Targeting fibrosis, mechanisms and clinical trials. Signal Transduct Target Ther 7, 206 (2022).
3. Wynn, T. A. & Ramalingam, T. R. Mechanisms of fibrosis: therapeutic translation for fibrotic disease. Nat Med 18, 1028–1040 (2012).
4. Van Linthout, S., Miteva, K. & Tschöpe, C. Crosstalk between fibroblasts and inflammatory cells. Cardiovascular Research vol. 102 258–269 (2014).
5. Lee, B., Lee, S. H. & Shin, K. Crosstalk between fibroblasts and T cells in immune networks. Frontiers in Immunology vol. 13 (2023).
6. Nicin, L., Wagner, J. U. G., Luxán, G. & Dimmeler, S. Fibroblast-mediated intercellular crosstalk in the healthy and diseased heart. FEBS Letters vol. 596 638–654 (2022).
7. Di, X. et al. Crosstalk between fibroblasts and immunocytes in fibrosis: From molecular mechanisms to clinical trials. Clin Transl Med 14, (2024).
8. Wilks, B. T., Evans, E. B., Nakhla, M. N. & Morgan, J. R. Directing fibroblast self-assembly to fabricate highly-aligned, collagen-rich matrices. Acta Biomater 81, 70–79 (2018).
9. Wilks, B. T. et al. Quantifying Cell-Derived Changes in Collagen Synthesis, Alignment, and Mechanics in a 3D Connective Tissue Model. Adv Sci (Weinh) 9, e2103939 (2022).
10. D. D. Cissell, J. M. Link, J. C. Hu, and K. A. Athanasiou, "A Modified Hydroxyproline Assay Based on Hydrochloric Acid in Ehrlich's Solution Accurately Measures Tissue Collagen Content," *Tissue Eng. - Part C Methods*, vol. 23, no. 4, pp. 243–250, 2017.

11. Hopkins, C. M., Wilks, B. T. & Morgan, J. R. TGF-β1 requires IL-13 to sustain collagen accumulation and increasing tissue strength and stiffness. Connect Tissue Res 66, 107–120 (2025).
12. Frangogiannis, N. Transforming growth factor-beta in tissue fibrosis. J Exp Med 217, e20190103 (2020).
13. Hinz, B. The extracellular matrix and transforming growth factor-beta1: Tale of a strained relationship. Matrix Biol 47, 54–65 (2015).
14. Shoulders, M. D. & Raines, R. T. Collagen structure and stability. Annu Rev Biochem 78, 929–958 (2009).
15. Hynes, R. O. The extracellular matrix: not just pretty fibrils. Science 326, 1216–1219 (2009).
16. Bose, P. Extracellular Matrix Architecture and Biomechanics of 3D Engineering Microtissues. (2018). https://doi.org/10.13140/RG.2.2.23413.83688
17. Ristaniemi, A., et al., Comparison of elastic, viscoelastic and failure tensile material properties of knee ligaments and patellar tendon. J Biomech, 2018. 79: p. 31-38.
18. Leask, A. & Abraham, D. J. TGF-beta signaling and the fibrotic response. FASEB J 18, 816–827 (2004).
19. Kouba, D. J. et al. Interferon-gamma and tumor necrosis factor-alpha act synergistically to inhibit type I collagen gene expression. J Invest Dermatol 111, 160–168 (1998).
20. Artlett, C. M. The role of the NLRP3 inflammasome in fibrosis. Open Rheumatol J 6, 80–86 (2012).
21. Gasse, P. et al. IL-1 and IL-23 mediate early IL-17A production in pulmonary inflammation leading to late fibrosis. PLoS ONE 6, e23185 (2011).

22. Ulloa, L., Doody, J. & Massagué, J. Inhibition of transforming growth factor-β/SMAD signalling by the interferon-γ/STAT pathway. Nature 397, 710–713 (1999).

23. Rider, P., Voronov, E., Dinarello, C. A., Apte, R. N. & Cohen, I. Alarmins: Feel the stress. J Immunol 198, 1395–1402 (2017).

24. Adebayo, O., Hookway, T. A., Hu, J. Z., Billiar, K. L. & Rolle, M. W. Self-assembled smooth muscle cell tissue rings exhibit greater tensile strength than cell-seeded fibrin or collagen gel rings. J Biomed Mater Res A 101, 428–437 (2013).

25. Gwyther, T. A. et al. Engineered vascular tissue fabricated from aggregated smooth muscle cells. Cells Tissues Organs 194, 13–24 (2011).

26. Dinarello, C. A., Novick, D., Kim, S. & Kaplanski, G. Interleukin-18 and IL-18 binding protein. Frontiers in Immunology vol. 4 (2013).

27. Sitia, R. & Rubartelli, A. The unconventional secretion of IL-1β: Handling a dangerous weapon to optimize inflammatory responses. Seminars in Cell and Developmental Biology vol. 83 12–21 (2018).

28. Landy, E., Carol, H., Ring, A. & Canna, S. Biological and clinical roles of IL-18 in inflammatory diseases. Nature Reviews Rheumatology vol. 20 33–47 (2024).

29. Pyrillou, K., Burzynski, L. C. & Clarke, M. C. H. Alternative Pathways of IL-1 Activation, and Its Role in Health and Disease. Frontiers in Immunology vol. 11 (2020).

30. Liu, Z.-G. The Molecular Mechanism of TNF Signaling and beyond. Cell Research vol. 15 (2005).

31. van Loo, G. & Bertrand, M. J. M. Death by TNF: a road to inflammation. Nature Reviews Immunology vol. 23 289–303 (2023).

32. Holbrook, J., Lara-Reyna, S., Jarosz-Griffiths, H. & McDermott, M. Tumour necrosis factor signalling in health and disease. F1000Research vol. 8 (2019).
33. Horiguchi, M., Ota, M. & Rifkin, D. B. Matrix control of transforming growth factor-beta function. J Biochem 152, 321–329 (2012).
34. Chen, C. Z. C. et al. The Scar-in-a-Jar: Studying potential antifibrotic compounds from the epigenetic to extracellular level in a single well. Br J Pharmacol 158, 1196–1209 (2009).
35. Coentro, J. Q. et al. Adapting the Scar-in-a-Jar to Skin Fibrosis and Screening Traditional and Contemporary Anti-Fibrotic Therapies. Front Bioeng Biotechnol 9, (2021).
36. Puerta Cavanzo, N., Bigaeva, E., Boersema, M., Olinga, P. & Bank, R. A. Macromolecular Crowding as a Tool to Screen Anti-fibrotic Drugs: The Scar-in-a-Jar System Revisited. Front Med (Lausanne) 7, (2021).
37. Skelly, D. A. et al. Single-Cell Transcriptional Profiling Reveals Cellular Diversity and Intercommunication in the Mouse Heart. Cell Rep 22, 600–610 (2018).
38. Xie, T. et al. Single-Cell Deconvolution of Fibroblast Heterogeneity in Mouse Pulmonary Fibrosis. Cell Rep 22, 3625–3640 (2018).
39. Plikus, M. V. et al. Fibroblasts: Origins, definitions, and functions in health and disease. Cell vol. 184 3852–3872 (2021).
40. Buechler, M. B. et al. Cross-tissue organization of the fibroblast lineage. Nature 593, 575–579 (2021).
41. Tsukui, T. et al. Collagen-producing lung cell atlas identifies multiple subsets with distinct localization and relevance to fibrosis. Nat Commun 11, (2020).

42. Lendahl, U., Muhl, L. & Betsholtz, C. Identification, discrimination and heterogeneity of fibroblasts. Nature Communications vol. 13 (2022).
43. Rieder, F. et al. Fibrosis: cross-organ biology and pathways to development of innovative drugs. Nature Reviews Drug Discovery vol. 24 543–569 (2025).
44. Martinez, F. J. et al. Idiopathic pulmonary fibrosis. Nature Reviews Disease Primers vol. 3 (2017).
45. Hinz, B., Phan, S. H., Thannickal, V. J., Galli, A., Bochaton-Piallat, M.-L. & Gabbiani, G. The myofibroblast: one function, multiple origins. Am J Pathol 170, 1807–1816 (2007).